05627-14-S

THE UNIVERSITY OF MICHIGAN

COLLEGE OF ENGINEERING
DEPARTMENT OF AEROSPACE ENGINEERING
HIGH ALTITUDE ENGINEERING LABORATORY

Scientific Report

The Current and Near-Fields of an Infinite Cylindrical Antenna Immersed in a Lossy Plasma Medium

EDMUND K. MILLER

Under contract with:

National Aeronautics and Space Administration
Contract No. NASr-54(05)
Washington, D. C.

Administered through:

December 1967

OFFICE OF RESEARCH ADMINISTRATION • ANN ARBOR

THE UNIVERSITY OF MICHIGAN

COLLEGE OF ENGINEERING

Department of Aerospace Engineering
High Altitude Engineering Laboratory

Scientific Report

THE CURRENT AND NEAR-FIELDS OF AN INFINITE CYLINDRICAL ANTENNA IMMERSED IN A LOSSY PLASMA MEDIUM

Edmund K. Miller

ORA Project 05627

under contract with:

NATIONAL AERONAUTICS AND SPACE ADMINISTRATION

CONTRACT NO. NASr-54(05)

WASHINGTON, D. C.

administered through:

OFFICE OF RESEARCH ADMINISTRATION ANN ARBOR

December 1967

TABLE OF CONTENTS

List of Figures

Abstract

The surface currents and near fields of an infinite cylindrical dipole antenna excited at a circumferential gap of non zero thickness and immersed in a lossy plasma medium which may be in the general case both compressible and anisotropic, there being a static magnetic field parallel to the antenna axis, are numerically investigated. The analysis proceeds from the linearized fluid equations for the electrons (ion motion is neglected) together with Maxwell's equations, and attempts to account for the actual inhomogeneous ion sheath which forms about a body at floating potential in a warm plasma by including in some of the results a concentric free-space layer, or vacuum sheath, between the antenna and the external uniform plasma. Fourier integrals are obtained for the various field quantities involved and are in particular examined numerically for the antenna current and the near electric field for parameter values typical of the E region of the ionosphere.

It is found that above $f_t = \sqrt{f_p^2 + f_h^2}$, with f_p and f_h the electron plasma and cyclotron frequencies, and sufficiently below f_t (on the order of $f_t/2$), the antenna current is generally wavelike in the axial direction with a wave number K_E, where $K_E < K_{Eo}$ for $f > f_t$ and $K_E > K_{Eo}$ for $f < f_t$, with K_{Eo} the free space electromagnetic (EM) wave number. The exception to this is when the plasma is incompressible, isotropic and there is no sheath, where then below f_p the current is evanescent along the antenna axis. When the plasma is compressible, there is in addition above f_t a small component of surface current whose wave number is near K_P, the acoustical wave number, but this current is on the order of 10^{-4} or less of that component near K_E and is thus of negligible importance in determining the antenna admittance. In the intermediate range $f_t/2 \lesssim f < f_t$ there is no well defined wave behavior of the antenna

current, the current then being generally evanescent in the axial direction. The plasma compressibility, vacuum sheath and plasma anisotropy thus serve to open up a region of antenna current wave propagation below f_t which vanishes when these three factors are all absent.

The plasma compressibility is also found to lead to EM and acoustical electrical fields at f_p which are two or three orders of magnitude larger than the corresponding values just above or below f_p, but which are of nearly equal magnitude and opposite sign so that the total field amplitude is relatively insensitive to the changing frequency, as f passes through f_p. Because of the large EM to acoustical propagation velocity ratio, it appears that the total electric field near an antenna pulsed at $f = f_p$ in a compressible plasma may remain large or even initially increase in value when the antenna excitation is removed, thus providing some insight into the relaxation resonance that has been observed with antennas in the ionosphere.

I. Introduction

The admittance of an infinite, cylindrical dipole antenna excited at a circumferential gap of non-zero thickness and immersed in a plasma medium has been the subject of attention in a recent series of reports (Miller, 1967a; 1967b; 1967c). These reports, which we will denote by I, II, and III respectively, deal with, in order, a compressible isotropic plasma, an incompressible anisotropic plasma and a compressible magnetoplasma as the medium in which the infinite antenna is immersed. This study was begun in order to gain some insight into the relative importance of the various factors which may affect the admittance of an antenna in an ionospheric-like plasma medium, such as acoustical and sheath effects arising from the non-zero plasma temperature, and the plasma anisotropy which results from the static ionospheric magnetic field. The ultimate goal of this study was to exploit the theoretical findings in the design, application and interpretation of experimental methods utilizing radio frequency antennas as diagnostic tools for ionospheric measurements.

It is apparent that the infinite antenna model, from the view point of conforming to the realities of the desired goal involving an actual antenna in the ionospheric plasma, is far from ideal. It has the distinct advantage however, that the theoretical ananysis may be formulated as a boundary value problem which includes without too great a complexity the important physical aspects of the plasma of greatest interest. At the same time the exciting source, a known voltage applied across the exciting gap, appears to be a physically more realistic assumption than that most often used in compressible plasma problems, a specified current distribution. An assumption implicit in performing the infinite antenna analysis to learn something about the finite antenna is that the medium influence on the infinite antenna and actual finite antenna will be similar. Thus while the infinite antenna approach cannot directly answer questions such as,

for example, the medium influence on the effect of changing antenna length, it may be successful in showing the gross variations of antenna admittance due to changing the various plasma parameters.

In addition to hopefully shedding some light on the admittance dependence of the finite antenna on the plasma properties, a solution for the infinite antenna current may be of more direct use in a theoretical study of the finite antenna admittance. This is because the finite cylindrical antenna may be regarded as a truncated infinitely long uniform system. As a result of truncating the infinite antenna to finite length, there will be multiply reflected current waves on the finite antenna similar to those on the infinite antenna. This approach has been used by Chen and Keller (1962), and Hallen (1963) for free space, and suggested as a possible technique by Lee and Lo (1967) for the incompressible magnetoplasma.

The purpose of this report is to discuss in greater detail the current waves on the infinite antenna for the plasma models treated in I, II and III. Some attention will also be devoted to the antenna near field.

II. Theoretical Considerations

(a) General Approach

The formulation of the infinite antenna problem begins with Maxwell's equations together with the linearized fluid equations of motion for the magnetoplasma, which may involve an electron pressure term if the plasma is compressible. The solutions to these equations are obtained in the usual way by the separation of variables. Because of the symmetry of the problem in the cylindrical coordinate (ρ, φ , z) system used, where the antenna axis and z-axis are coincident, the solutions are dependent upon ρ and z only.

The various physical quantities of interest such as the electric and magnetic fields, electron velocity, etc. may be obtained from the z-components of the electric and magnetic fields as well as the dynamic electron density, in the case of the compressible plasma. These three quantities thus serve as potentials which yield the remaining field variables. The potentials are expressed formally as a Fourier integral over the z-direction separation constant, β , of the product of the radial-direction solution given by a Hankel function whose argument involves the product of ρ times the appropriate radial separation constant, and the Fourier amplitude of the potential. Since the transformed field quantities in the ρ, β space satisfy the Fourier transforms of the boundary condition equations in ρ, z space, the Fourier potential amplitudes are obtained from a matrix formed by the transformed boundary condition equations.

This procedure is well known, and the details are given in some detail in I thru III. It may be remarked that considerably increased complexity results in the case of the compressible magnetoplasma, but the basic approach is the same. The problem is of course that once the Fourier potential amplitudes have been obtained, it is necessary to invert the appropriate Fourier

integral to find a desired field quantity. Unfortunately, because of the complex character of the kernel of the Fourier integral, it is not possible to obtain an analytic solution for the field quantity, except possibly for some special cases. Consequently, beyond the point of formally finding the analytic form of the kernel of the Fourier integral, we are limited to numerical computations for investigating various quantities of interest.

The details of this latter step are recounted at length in I through III. Since the quantity of primary interest in these reports is the infinite antenna admittance, which is found from the axial antenna current at the exciting gap, the discussion of the numerical approach used, and the results which are presented in I through III are confined almost entirely to the antenna admittance. While this approach has been satisfactory in view of our concern with the infinite antenna admittance as the physically most significant quantity to be obtained from the analysis, it ignores much other potentially useful information that could also be obtained about the antenna fields and currents. (This neglect of emphasis on the antenna fields and currents in favor of the admittance is also dictated by economic considerations of the computer time required for the calculations of the former compared with the latter, as will be made clearer in the subsequent discussion.)

In spite of the limitations which are imposed on a thorough numerical investigation of the fields and currents, some limited calculations of these quantities have been performed. In addition, the computer output which was produced in the course of the admittance calculations has provided valuable information about the antenna current waves. The next section describes the manner by which the numerical results to be presented have been obtained.

(b) Method of Calculation

The starting point for the numerical analysis followed in this study is the Fourier integral for the antenna admittance, which may be written, with δ the exciting gap thickness,

$$Y = G + i\,B \qquad (1)$$

$$= I_z(z=\delta/2)$$

$$= \int_0^\infty \cos(\beta z)\; i_z(\beta)\, d\beta \;\Big|_{z=\delta/2}$$

$$= 2\pi c \int_0^\infty \cos(\beta z)\; h_\varphi(\beta, \rho=c)\, d\beta \;\Big|_{z=\delta/2}$$

Since the assumed source is unit excitation voltage applied across the exciting gap and varying as $e^{i\omega t}$, all the quantities in (1) are implicit function of ω. The antenna admittance, conductance and susceptance are denoted respectively by Y, G, and B, with I_z the axial antenna current. The Fourier transforms in β-space of functions denoted by upper case letters in coordinate space are shown by lower case letters. The axial current is seen to be given by $2\pi c$ times the φ-component of magnetic field evaluated at $\rho=c$ with c the antenna radius. It is obvious that the analytic form of $h_\varphi(\beta, \rho)$ will depend on the sheath-plasma model used in the analysis. Since $h_\varphi(\beta, \rho)$ becomes very complicated for the anisotropic plasma, the explicit form of $h_\varphi(\beta, \rho)$ is given in I through III for only the isotropic case, a numerical matrix inversion having been used to find $h_\varphi(\beta, \rho)$ for the anisotropic case.

A factor appcars in the transforms of all the field quantities which is the "form factor" or spatial frequency spectrum in β-space of the assumed source, which is

$$S(\beta) = \frac{\sin(\beta\,\delta/2)}{(\beta\,\delta/2)} \qquad (2)$$

If the exciting gap is of zero thickness, an approximation sometimes employed in antenna theory, then it may be shown that the antenna current is infinite at the gap, i.e., the integral in (1) does not converge for $\delta = 0$. This is also the case for the z-component of electric field. The inclusion of a non-zero exciting gap thickness, besides being more reasonable on physical grounds than zero gap thickness, is required if the interpretation of the antenna admittance is to be unambiguous.

The difficulty of numerically evaluating the integral of Eq. (1) is due for the most part, aside from the problem of obtaining a numerical value for the integrand function, to the location of an infinity in the integrand, which for the case of zero electron collision frequency, may lie on the real β-axis. If the infinity does lie on the path of integration, the improper integral may be attacked directly by defining the admittance by the principal value of the improper integral. An alternative method that could be employed is a deformation of the integration path around the singularity. This has been done in obtaining the infinite antenna free-space admittance reported on in I. Perhaps the easist way to handle this problem however is to employ a non-zero electron collision frequency to remove the infinity from the real β-axis. At the same time, the problem is made more realistic since at least in the lower ionosphere, the electron collision frequency is not negligible compared with the electron plasma frequency. It should be mentioned that the real and imaginary parts of (1) have different kinds of infinities, the imaginary part having infinities of opposite sign on either side of the singular point, while the real part does not change sign, for zero collision frequency. When there is a non-zero collision frequency, the real part of (1) may instead by sharply peaked but of finite value, while the imaginary part has finite peaks of opposite sign on either side of, and is zero at, some value of β.

While the non-zero electron collision frequency does remove the integrand infinity from the real β-axis, the integrand may still increase typically by several orders of magnitude in its vicinity, for the collision frequency values used in these calculations. In order to economically and accurately integrate such a function it is necessary to greatly compress the number of calculated points in the peaks compared with the region outside. An integration routine which does this was developed, and provides a convergence check at each point of the numerical integration, based on the Romberg technique; it is discussed in detail in I.

Besides the integrand peak just discussed, there are other considerations to be taken into account in numerically evaluating an integral of the kind shown in (1). Because of the $\cos(\beta z)$ term, the integrand will exhibit an oscillatory behavior with β. For the value of z used when Y is to be calculated, $\delta/2$, this oscillatory behavior does not become significant until $\beta \sim \delta^{-1}$. However, since the major contribution to the integral comes from β values orders of magnitude less than this, for the gap thickness used in the study, then the oscillation of the integrand due to $\cos(\beta z)$ is not a factor of importance when calculating the admittance.

If however, the current is to be calculated as a function of z, in order to investigate the current waves on the antenna, then the onset of oscillatory integrand behavior due to the $\cos(\beta z)$ term occurs approximately when $\beta \sim z^{-1}$. Thus, the larger the value of z for which the current is required, the smaller the β value where the integrand oscillation begins. The problem which arises from this is that the numerical integration of an oscillatory function requires a minimum of roughly six integrand values per cycle in order to be accurately evaluated. For large z then, this consideration becomes important in establishing the number of integrand evaluations required for the numerical integration,

with the spacing along the β -axis going approximately as $\pi/6z$. It may be added that a similar consideration applies when the various field quantities are to be calculated as a function of the radial variable ρ, the oscillatory behavior then arising from a Hankel function whose argument contains ρ, which is a factor in the transformed field quantities.

The difficulty which is encountered then when we want to calculate the current along the antenna or the field variation with z and ρ is that the number of integrand evaluations required may become very large compared with those needed for determining the admittance alone, and the sequence of abscissa values required may vary with both z and ρ. Because the most time consuming part of the integration is the integrand evaluation, this means that when z and/or ρ are large enough, each field value obtained may require substantially more computer time than does an admittance calculation. When it is noted that the admittance calculations require from 30 seconds to 6 minutes or more each of computer time (IBM 7090) depending on the plasma model used, it becomes obvious that a systematic field and current calculation is not practical.

If the constraint is accepted then that integrand evaluations are to be made for only the sequence of abscissa values required for the admittance calculation, it may still be possible to carry out a limited investigation of the antenna fields and current. The results to be obtained in this way would be roughly limited to z and ρ values where the abscissa spacing in the integrand peaks, or regions of greatest contribution to the integral, are on the order of $\pi/6z$ or $\pi/6\rho$, or smaller. Since, also roughly speaking, the abscissa spacing in the integrand peak was found to be about 10^{-2} the value of β at its center, which we denote here as β_o, then the largest ρ or z value that can be used would be given by

$$x \sim 50\ \beta_o^{-1} \tag{3}$$

where x represents ρ or z. This spacing in β was typically required for a normalized convergence accuracy in the integration of 10^{-4}. If there is an appreciable contribution to the integral from the β-range outside the peak, then the range of z or ρ that may be investigated can be very much reduced from that indicated by (3), which thus represents a very optimistic upper limit on z or ρ.

Even with the limitations thus imposed on the field and current calculations, some meaningful results can be obtained using the approach outlined above. The more significant of these are included in the next section. It should be mentioned that these calculations have been done for the isotropic plasma model only. The same calculations for the anisotropic case would have required a considerable modification of the computer programs written for the admittance due to the storage requirements exceeding the computer capacity.

While a direct calculation of the fields and current has been somewhat limited, there is some potentially very useful information contained in the sequence of abscissa values used for the integration, and the corresponding integrand values. It was mentioned above that for zero electron collision frequency, an integrand infinity may be located on the real β-axis. This infinity arises because the integrand denominator goes to zero. The integrand denominator is given by the determinant of the Fourier coefficient matrix established by the boundary condition equations. This type of determinant zero is well known as providing a solution for the free oscillations which may occur in boundary value problems. When the determinant, which we denote by D, is set equal to zero to provide an expression for the β at which these free oscillations occur, the equation $D(\beta)=0$ is called a characteristic equation and the solutions for β may be called characteristic roots, or characteristic wave numbers. The abscissa and integrand values obtained then in the course of evaluating

(1), (and which are produced as output by the computer routine) would thus be capable of providing under certain conditions the characteristic wave numbers when the collision frequency is zero.

The advantage of finding the characteristic waves which may propagate on the infinite antenna is twofold. First, the effect of the plasma and sheath on the characteristic waves may provide pertinent information about the relative effects of the various physical processes being investigated. Second, from the viewpoint of using the infinite antenna current to investigate the truncated or finite antenna current, the contribution to the total infinite antenna current coming from the characteristic wave is of importance in determining the wavelike nature of the infinite antenna current and the implications of this for the finite antenna, in terms of resonant antenna length, etc. Thus, if the current at the exciting gap of the infinite antenna comes for the most part from a peak centered at β_o, then the current variation with z will be given by $\cos(\beta_o z)$, i.e., the characteristic wave acts very nearly as an impluse or delta-function centered at β_o.

While the preceding discussion has been concerned with the zero collision frequency situation, the actual calculations were carried out for a non-zero collision frequency. Since the value used for the electron collision frequency in the calculations is on the order of 10^{-3} times the radian electron plasma frequency, the characteristic wave solution obtained in this case should not be too much different from that found in the collisionless case.

This cannot be verified analytically in general, since the characteristic wave number must be obtained by numerical means, but for the sheathless, incompressible magnetoplasma, an analytic expression for the characteristic wave number can be obtained for the case of vanishing cylinder radius and is given by (Lee and Lo, 1967)

$$\beta_o = \pm\sqrt{1 - \frac{UN^2}{U^2-H^2}} \tag{4}$$

where

$$U = 1 - i\,\nu/\omega$$
$$N^2 = \omega_p^2/\omega^2 = f_p^2 / f^2$$
$$H = f_h / f$$

The electron collision, cyclotron and plasma frequencies are denoted by ν, f_h and f_p respectively. We see that when $\nu/\omega \ll 1$, β_o may be written

$$\beta_o \approx \pm\sqrt{1 - \frac{N^2}{1-H^2}\left[1 + \frac{i\,\nu}{\omega}\left(\frac{1+H^2}{1-H^2}\right)\right]} \tag{5}$$

so that a solution for β_o for non-zero collision frequency is of practically the same amplitude but slightly different in phase compared with that for the collisionless case. Depending on the values of N^2 and H, β_o will be for this case almost pure real of pure imaginary.

An obvious limitation of the numerical approach described above for finding the characteristic wave solution is that since the integration path is the real β-axis, the complex wave number is not established. The numerical method used then, involving as it does the integrand values required for the numerical integration, is capable of providing only the real component of the characteristic wave number and then only for the case where β_o is almost pure real. In view of our interest in the characteristic wave number as showing the wavelike behavior of the infinite antenna current, this is not too serious a limitation however, since an imaginary β_o would be an indication of a characteristic wave which is evanescent in the z-direction. The real part of β_o obtained from this approach will be denoted by K_{zr} in the following. The existence of a complex wave number solution is discussed more fully in section (c) below.

It is apparent that having found the real part of the characteristic wave number for a given situation, the infinite antenna current cannot be concluded to exhibit a simple wave-like behavior associated with this wave number.

The relative contribution to the total current at the exciting gap coming from the peak at this wave number will determine this.

Thus, in presenting the results for K_{zr} in the following, we will also show the ratio of the real component of the antenna current at the exciting gap coming from the integration range $\beta = 0.9\ K_{zr}$ to $\beta = 1.1\ K_{zr}$ to the total real current coming from $\beta = 0$ to $\beta = \infty$. If this ratio is near unity, then, the z behavior of the antenna current will be nearly $\cos(K_{zr}z)$. Besides finding the characteristic wave number then, the relative contribution to the total current arising from the peak and the consequent wave-like behavior of the total antenna current may be demonstrated. The imaginary antenna current is not so suited to this purpose since it has a zero at K_{zr} with a negative maximum just below and a positive maximum just above K_{zr}. Some graphs of the calculated current as a function of z will be included in the results so that the applicability of the approach outlined above may be shown.

Finally, in order to more clearly show the dependence of K_{zr} on the various plasma parameters, some graphs of the real part of the integrand function as a function of β will be shown. Such curves will also show the widths of the current peaks which occur as β varies and graphically illustrate the problems encountered in a numerical integration of the Fourier current integral.

(c) The possibility for complex wave numbers when the collision frequency is zero.

The discussion above concerning the characteristic wave number implies, but does not state so explicitly, that when the electron collision frequency is zero the wave number will be pure real or pure imaginary. To a large extent this is only approximately true, and is exact only for the case of the isotropic, incompressible plasma. When the plasma is anisotropic and/or compressible, the characteristic wave solutions may in some cases be nearly, but not exactly, pure real or pure imaginary.

To cite a specific example, we may consider again the sheathless, incompressible, anisotropic plasma for which Lee and Lo (1967) obtained the characteristic solution for the case of vanishing cylinder radius, as given by (4) above. Their solution for β_o shows that whenever $f>f_t$ or $f<f_h$, and f_p, the solution for β_o is pure real, it being otherwise pure imaginary. Seshadri (1965) performed some calculations to solve the characteristic equation for this particular case and found on the other hand that β_o is complex except when $f< f_h$ and f_p where it is pure real.

The answer to this discrepancy appears to be that Lee and Lo consider the case of vanishing cylinder radius, where it then becomes possible to replace in the characteristic equation the ratio of two Hankel functions of order zero whose arguments are proportional to c, the cylinder radius, by unity. For non zero radius however, this ratio is complex. Consequently, while in the former case the characteristic equation $D(\beta) = 0$ has only pure real coefficients, and so yields a pure real or imaginary solution, in the latter case, it is complex and so has a complex solution.

A somewhat analogous situation arises in the case of the compressible, isotropic plasma, when $f>f_p$. In this case, a pure real solution is found which is in magnitude on the order of the plane wave EK propagation constant. A second

solution is found near the EM plane wave propagation constant, but it is complex, rather than pure real, except in the limit of vanishing cylinder radius. This is discussed in Appendix C, where the characteristic wave solutions are examined for the various plasma models considered in this report.

The conclusion to be drawn from this property of the characteristic wave numbers when the plasma is compressible or anisotropic is that the non-zero cylinder radius may result in axially decaying characteristic or free waves, propagating along the cylinder. This may occur above f_t or f_p and in the absence of electron collisions. (This effect of the non-zero cylinder radius upon the antenna conductance, and thus the power supplied by the source to the plasma, is very similar to that which is found to take place when the plasma is isotropic and incompressible, but has a non-zero electron collision frequency.) The fields at the characteristic wave number may be evanescent in the radial direction (as discussed in Appendix C), but for somewhat smaller β values, where the contrbution to the antenna current from the peak centered at the characteristic wave number may still be significant, they are radially propagating.

It may be seen then that the plasma compressibility and anisotropy may produce some rather subtle effects, particularly when the characteristic waves that may propagate along an infinite cylinder are considered. If the investigation is confined to considering for example, the pure real characteristic wave numbers for the isotropic, compressible plasma, as Cook and Edgar (1966) díd, the results may mislead to overemphasizing the importance of the characteristic wave corresponding to the EK propagation constant. The results obtained by Cook and Edgar would lead to the conclusion that the plasma compressibility is very influential in determining the current on the infinite antenna, whereas it was established in I that just the opposite is the case. The important point is that in order to analyze the current flowing on an infinite cylinder, the entire problem, including the exciting source, must be considered to place the various factors involved in their proper perspective. This should be made clearer with the results to be given in the next section, particularly the graphs of the integrand as a function of β.

III. Numerical Results

The results to be presented here are extracted for the most part from the computer output produced in the course of obtaining the infinite antenna admittance values presented in I through III. An exception to this are the field and current values for which some additional calculations were required. Because of the variety of the results which follow, an attempt has been made to present them in a logical sequence, the results being grouped according to kind rather than by the plasma model used. This has the advantage that the effect on a given quantity of changing the various plasma parameters may be more readily appreciated. The order of presentation is: (a) Integrand variation as a function of β ; (b) The real wave number K_{zr} as a function of frequency; (c) The ratio of the peak contribution to the total real current; (d) Antenna current as a function of z; and (e) The antenna near-fields.

(a) Integrand variation as a function of β.

A graph of the integrand of (1) as a function of β may be much more revealing than the admittance, which is an averaged quantity, in demonstrating the role of the various plasma parameters as they influence the antenna currents. An example of this is shown in Figs. 1 and 2 which present the real component of the integrand of (1), denoted by $i_R(\beta)$, as a function of β, for the isotropic plasma and both the sheathless and vacuum sheath models. Figure 1 is for an incompressible (the electron temperature $T=0^{\circ}K$) plasma, and Fig. 2 is for the compressible ($T=1,500^{\circ}K$) plasma (the EK wave is excited then), with an antenna radius, c, of 1 cm, an exciting gap thickness, δ, of 0.1 cm, electron plasma and collision frequencies of 1.5MHz and $10^4 sec^{-1}$, and an exciting frequency of 2.0MHz. These results are obtained for a perfectly reflecting, or rigid, boundary at the plasma-sheath or plasma-cylinder, interface, for the incident electrons.

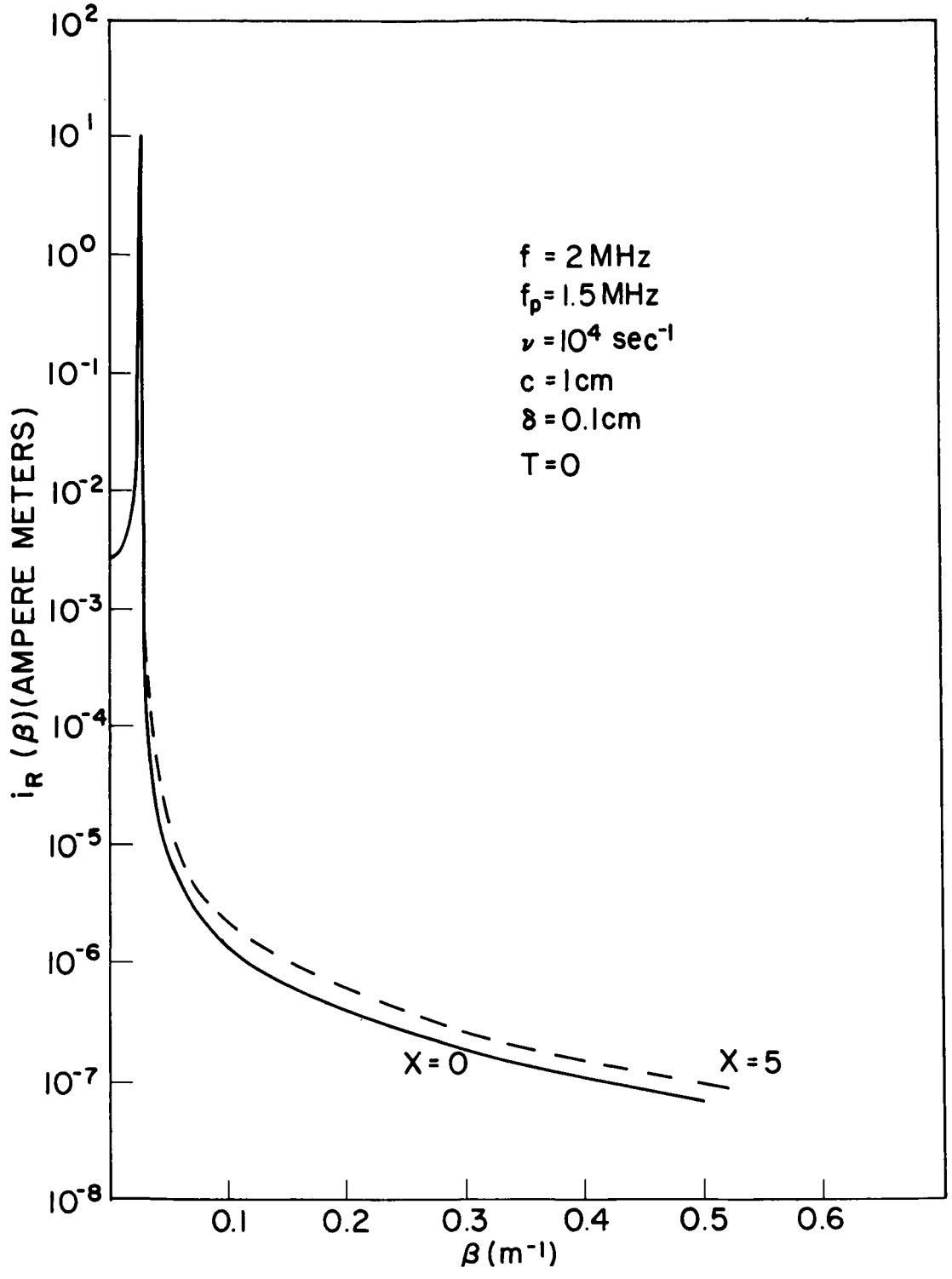

Fig. 1. The real Fourier component of the infinite antenna current $i_R(\beta)$ as a function of β for the incompressible, isotropic plasma and the sheathless and 5 Debye length vacuum sheath cases.

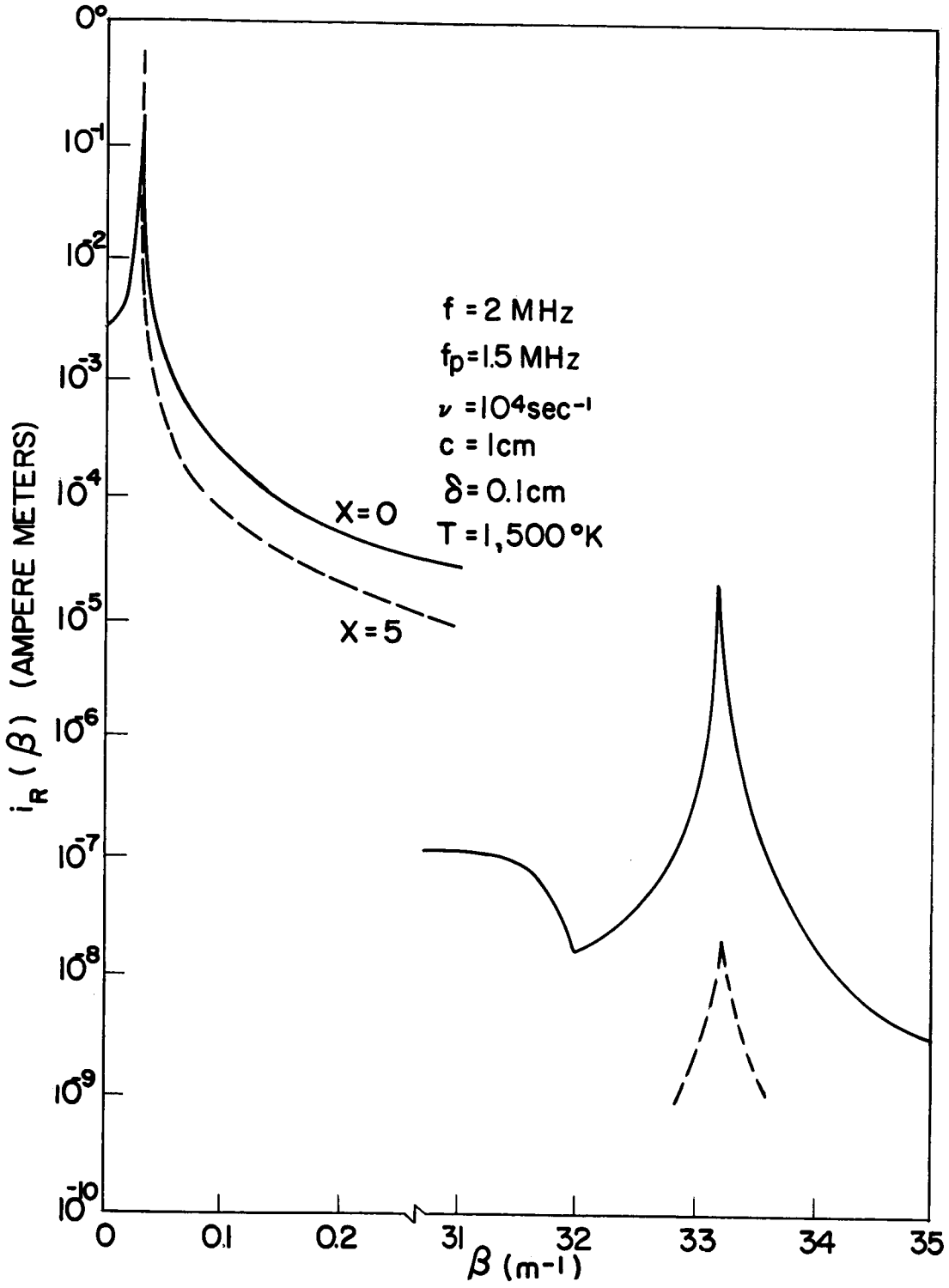

Fig. 2. The real Fourier current component $i_R(\beta)$ as a function of β for the compressible, isotropic plasma and the sheathless and 5 Debye length vacuum sheath cases.

The sheath thickness for the vacuum sheath case is 0.0799 m equal to 5 electron Debye lengths (D_ℓ) for an electron temperature of 1, 500°K and is denoted by X measured in units of D_ℓ on these and subsequent graphs. Note that

$$D_\ell = \sqrt{kT/m} \quad /\omega_p \tag{6}$$

where k is Boltzmann's constant and m is the electron mass. We thus regard the electron temperature for calculating the sheath thickness and that used for the compressible plasma temperature as independent quantities so that the sheath and compressibility effects may be separated. Unless otherwise indicated, the temperature used to calculate D_ℓ will be 1, 500°K.

Figures 1 and 2 are similar in that each set of curves exhibits a maximum in $i_R(\beta)$ at about $\beta = 0.028\ m^{-1}$. This corresponds to the wave number of an EM wave in a plasma medium whose relative dielectric constant is, for small electron collision frequency,

$$\epsilon_r = (1 - N^2) \tag{7}$$

and the wave number of the EM wave is

$$K_E = \frac{\omega}{v_\ell}\sqrt{\epsilon_r} = K_{Eo}\sqrt{\epsilon_r} \tag{8}$$

where v_ℓ is the free space velocity of light. Calculating K_E from (8) yields $K_E = 0.0285$ which agrees with the peak in $i_R(\beta)$ of Figs. 1 and 2. It may be seen that on both graphs, the sheathless case peak values of i_R are less, but fall off more slowly than the corresponding vacuum sheath curves.

The compressible results of Fig. 2 exhibit in addition to the peak at $\beta = K_E$, another peak at about $\beta = 33.2$. The EK wave number in the plasma medium, again for small electron collision frequency, is

$$K_P = \frac{\omega}{v_r}\sqrt{\epsilon_r} = K_{Po}\sqrt{\epsilon_r} \tag{9}$$

where v_r is the rms thermal electron velocity. The value for K_P obtained from (9) is $K_P = 33.1\ m^{-1}$, again in agreement with the peak in $i_R(\beta)$.

We see that for the compressible plasma then, two distinct characteristic waves, or surface current waves, are excited, one the EM mode, and the other the EK mode. The EK mode current is about 4 orders of magnitude less than the EM mode current for the sheathless case, while the addition of the sheath increases the difference to about 7 orders of magnitude. Thus, while the source may excite a current wave on the antenna with the EK wave number, it has little effect on the total current which is dominated by the EM contribution. It should be mentioned that the EK mode is not produced at all, if the rigid boundary condition used for these calculations is replaced by a perfectly absorbing, or soft boundary (see Miller, 1967a). Also, the use of Balmain's (1966) absorptive boundary condition effectively decouples the antenna from the EK mode, leading to the same results as the soft boundary. This is discussed in Appendix A.

It is obvious upon seeing the results of Figs. 1 and 2 that if only the pure real characteristic wave numbers are sought, then because the wave number near K_E for the compressible plasma is complex (for both the sheathless and vacuum sheath cases), the predominant wave-like behavior of the antenna current may be thought to be on the order of K_P. As indicated by Fig. 2, and as will be subsequently shown directly in showing the antenna current as a function of z, the total current varies more nearly with the wave number K_E, with only a small superimposed ripple due to the current contribution from the peak near K_P. Because the peak at K_P is more sensitive to the electron collision frequency than is the peak at K_E, we will also show below the result of changing the collision frequency on the curve for the sheathless case of Fig. 2, in order to see whether the peak at K_P may become dominant with vanishing collision frequency.

It is interesting to note that the infinite antenna conductance, which comes from integrating the $i_R(\beta)$ curves such as shown in Figs. 1 and 2 does not differ by more than 5 percent for the four cases considered. Thus, the conductance, as mentioned, tends to average out what are significant features in $i_R(\beta)$, as shown by Figs. 1 and 2.

Fig. 3 shows $i_R(\beta)$ for the sheathless case with the electron temperature a parameter, and a frequency f of 1.4 MHz, the other parameter values being the same as for Figs. 1 and 2. The $T = 0^{\circ}K$ curve alone has no peak, with the other curves exhibiting peaks in $i_R(\beta)$ that shift to lower values of β with increasing electron temperature. The plasma compressibility due to the non-zero electron temperatures thus has the effect of causing a surface current wave to be excited. It is of interest to note that the conductance is a not very sensitive function of the electron temperature, for the value of electron collision frequency used here, though the curves of $i_R(\beta)$ for the various temperatures are quite different. This is discussed in more detail in I. A small peak may be seen near $\beta = 0$ in the $i_R(\beta)$ curves; this does not appear to be associated with a characteristic wave solution as the imaginary current component, $i_I(\beta)$, does not change sign there, nor is the peak height a function of collision frequency.

The vacuum sheath thickness, X, is a parameter on Figs. 4 and 5 which present $i_R(\beta)$ for the incompressible and compressible plasma respectively, for a frequency of 1 MHz and the other parameter values remaining the same as for the previous figures. A comparison of Figs. 3 and 4 reveals that increasing the vacuum sheath thickness for the incompressible plasma has a very similar effect to increasing the electron temperature for the sheathless, compressible plasma. A similar effect has been remarked on in I where the vacuum sheath and plasma compressibility were found to influence the antenna admittance in much the same way.

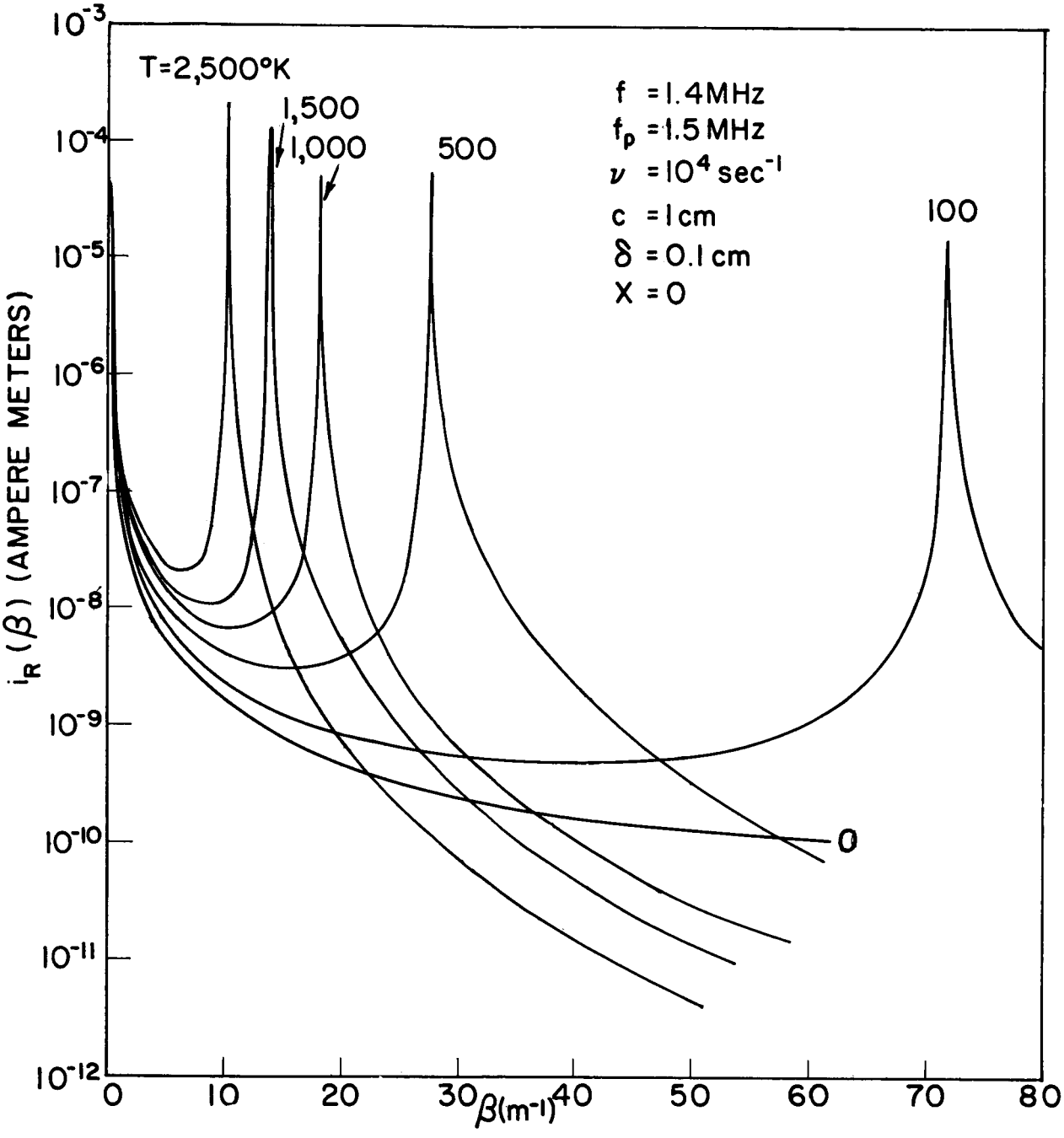

Fig. 3. The real Fourier current component $i_R(\beta)$ as a function of β for the sheathless, isotropic compressible plasma with the electron temperature T a parameter.

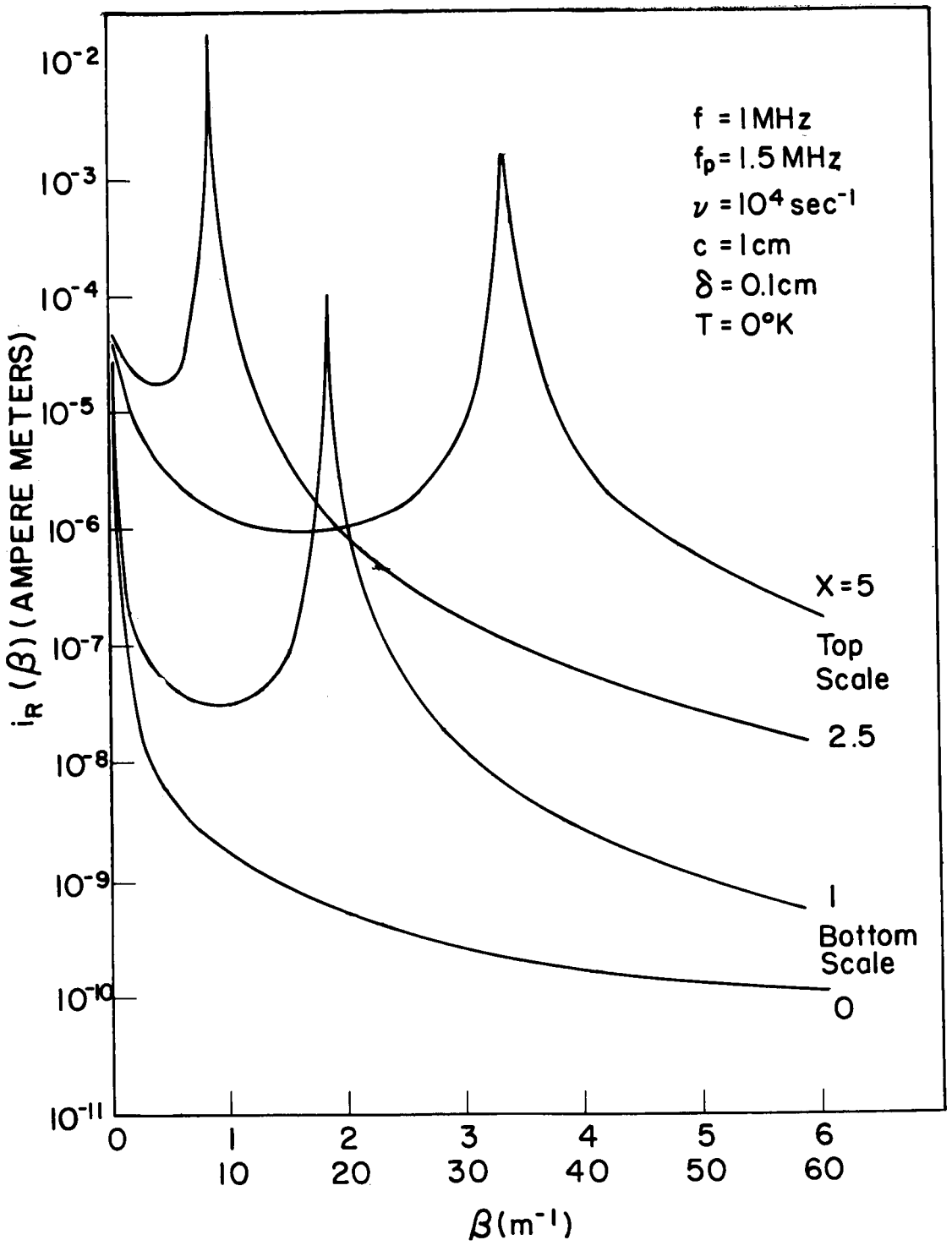

Fig. 4. The real Fourier current component $i_R(\beta)$ as a function of β for the isotropic, incompressible plasma with the vacuum sheath thickness X a parameter.

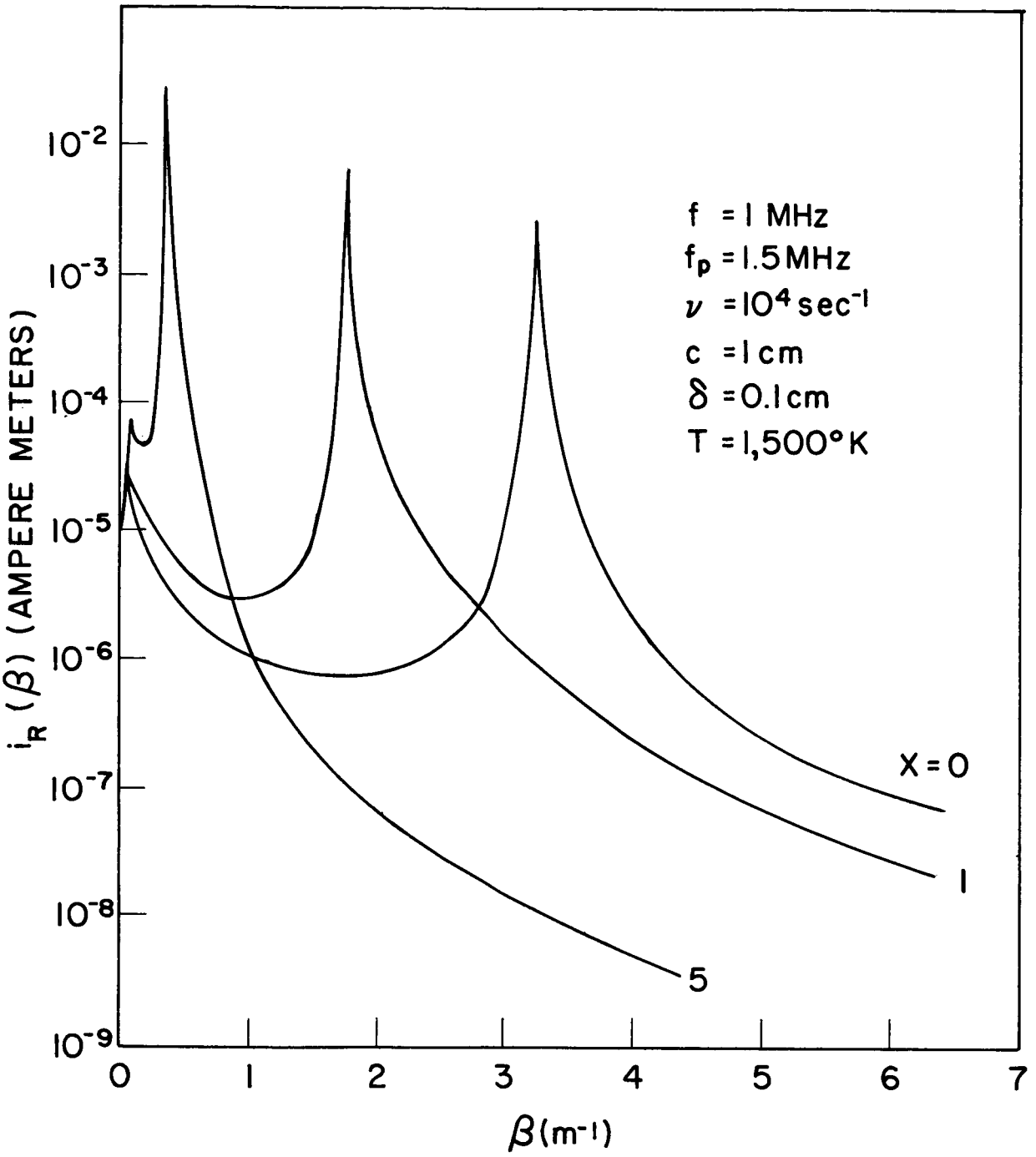

Fig. 5. The real Fourier current component $i_R(\beta)$ as a function of β for the isotropic, compressible plasma with the vacuum sheath thickness X a parameter.

The vacuum sheath may be observed in Fig. 5 to also decrease the value of β at which the peak in $i_R(\beta)$ occurs for the compressible plasma. The sensitivity of the peak location of $i_R(\beta)$ to X is seen to be less for the compressible case of Fig. 5 than the incompressible case of Fig. 4. When X becomes large enough however, the difference between $i_R(\beta)$ for the compressible and incompressible plasma becomes less. This feature is also exhibited by the antenna admittance . It thus appears that the effect of plasma compressibility on the admittance and antenna current is significantly decreased, and that the EK wave may be effectively decoupled from the plasma, by the vacuum sheath.

We present $i_R(\beta)$ in Figs. 6 and 7 for the sheathless case, and the incompressible and compressible plasmas respectively, with the collision frequency a parameter. The other parameter values are the same as for the previous graphs with the exception of f, which is 1.4 MHz. The results of Fig. 6 for the incompressible case have no peak in $i_R(\beta)$ except the small increase near $\beta=0$ discussed previously. In addition the magnitudes of the $i_R(\beta)$ curves of Fig. 6 are seen to be proportional to ν, with the result that the conductance is also linearly proportional to ν. This is as expected, since the conductance in the incompressible, sheathless plasma is zero below the plasma frequency when the electron collision frequency is zero. It is also interesting to note that since the $i_R(\beta)$ curve varies approximately as $(\beta^2+a^2)^{-1}$ on Fig. 6, the z-variation of the real current component at least, will be generally evanescent, since

$$\int_0^\infty \frac{\cos \beta z}{\beta^2+a^2}\, d\beta \propto \frac{\pi e^{-za}}{2a}$$

This will be verified to be the case when the current variation with z is given in section III d.

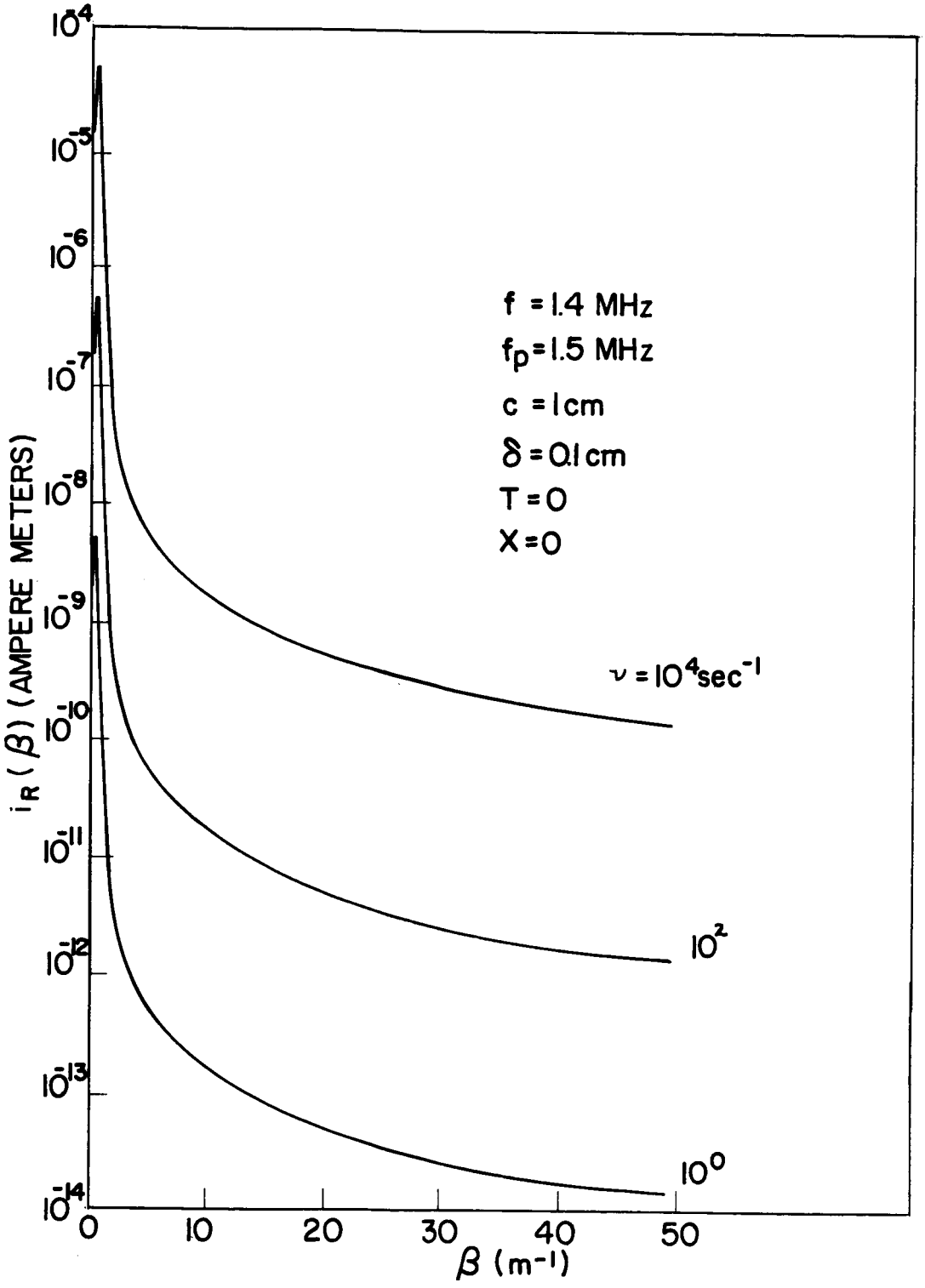

Fig. 6. The real Fourier current component $i_R(\beta)$ as a function of β for the isotropic, incompressible plasma with the electron collision frequency ν a parameter and $f < f_p$.

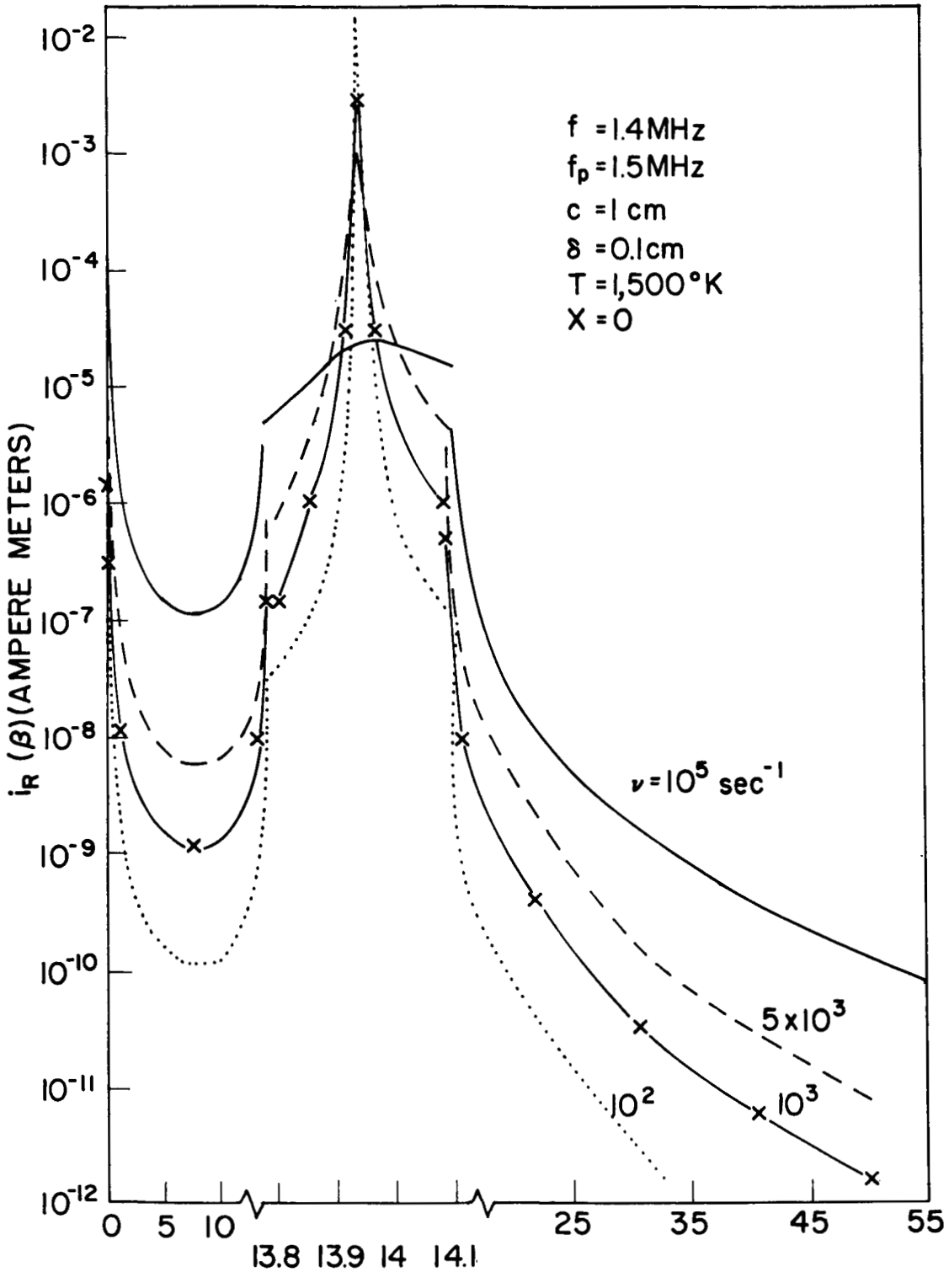

Fig. 7. The real Fourier current component $i_R(\beta)$ as a function of β for the isotropic compressible plasma with the electron collision frequency ν a parameter and $f < f_p$.

In Fig. 7 however, where the compressible plasma is considered, a very different result is observed. The peak in $i_R(\beta)$ may be seen to increase in magnitude and decrease in width with decreasing ν with the result that the conductance is almost independent of ν, a phenomenon discussed more fully in I. Further, as ν is decreased, the proportion of the total current contributed by the peak appears to increase since the variation of $i_R(\beta)$ outside the peak is proportional to ν. Since the plasma is completely reactive below the plasma frequency for zero collision frequency, then in the absence of a sheath the conductance is expected to be zero. Thus, if the limit $\nu \longrightarrow 0$ is taken, then the width of the peak in $i_R(\beta)$ must eventually decrease towards zero more rapidly than the height approaches infinity, so that the integral of $i_R(\beta)$ approaches zero. The behavior of $i_R(\beta)$ is examined in Appendix B where the limit $\nu \rightarrow 0$ is considered, and the dependence of the conductance on the electron temperature and collision frequency for this limit is examined.

The results of varying the electron collision frequency for the incompressible plasma when there is no sheath is shown in Fig. 8 for the case where $f > f_p$, f now being 1.6 MHz, the other parameters having the values used for Fig. 6. There it may be seen that the peak in $i_R(\beta)$ increases in magnitude and decreases in width in inverse proportion to ν, so that the conductance is nearly independent of the collision frequency.

In Fig. 9 are shown the results for the compressible plasma and the sheathless case for various collision frequency values, and a frequency of 2MHz, with the other parameter values as used for Fig. 7. Here we see that for the compressible plasma, the peak near K_E is not affected by the changing values of collision frequency, while that near K_P decreases in width and increases in magnitude as β is decreased. When the collision frequency is made zero,

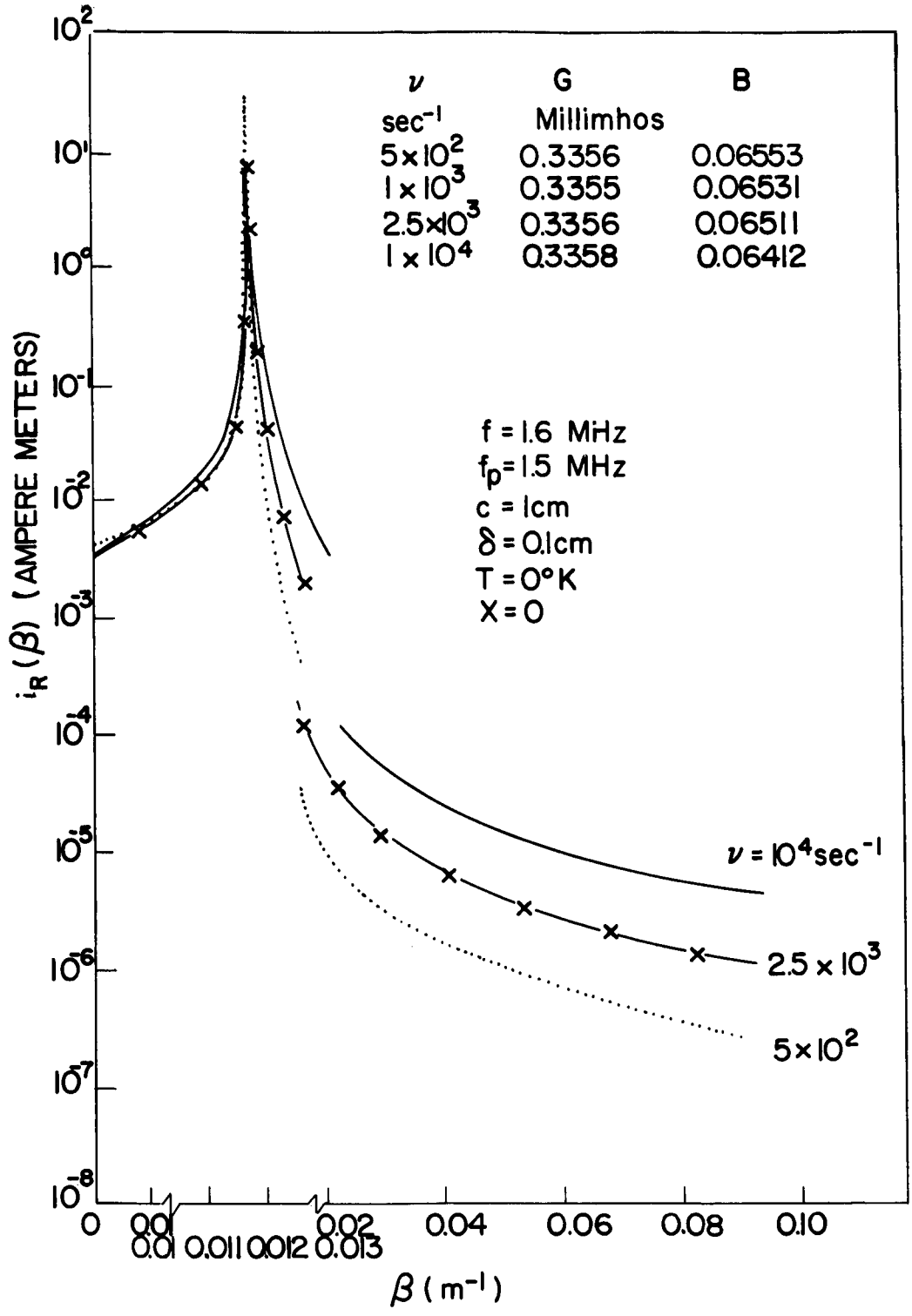

Fig. 8. The real Fourier current component $i_R(\beta)$ as a function of β for the isotropic, incompressible plasma with the electron collision frequency a parameter and $f > f_p$.

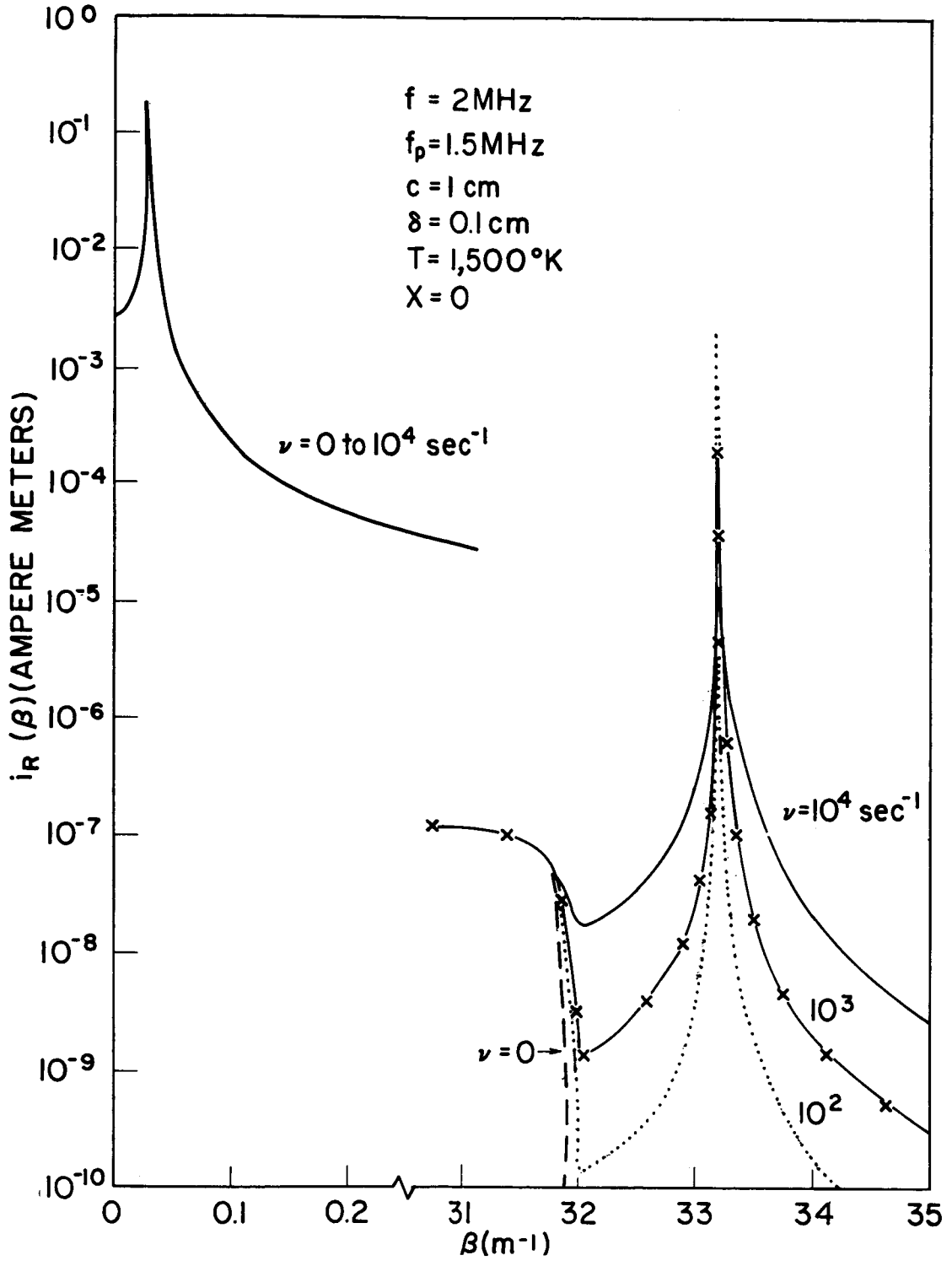

Fig. 9. The real Fourier current component $i_R(\beta)$ as a function of β for the isotropic, compressible plasma with the electron collision frequency a parameter and $f > f_p$.

then $i_R(\beta)$ has no peak near K_P, although the imaginary part, $i_I(\beta)$, becomes infinite then as discussed in Appendix B.

In the case of zero collision frequency, the admittance may be obtained by deforming the integration path. For purposes of comparison, the antenna conductance and susceptance are given in Table I for the sheathless, compressible plasma as a function of the collision frequency for f = 2MHz. Also given is the incompressible admittance. It may be seen that neither the conductance nor the susceptance is very sensitive to ν for the compressible plasma, even though the $i_R(\beta)$ curve does exhibit a considerable collision frequency dependence near K_P. The important point is that the admittance is due principally to the peak near K_E which is not affected by changing ν. It thus seems obvious that an analysis of the current on an infinite cylinder such as performed by Cook and Edgar (1966) which is concerned with only the characteristic waves with pure real wave numbers on the cylinder, is incapable of providing any real insight into the current on an antenna in a plasma because it ignores the more important current contribution from the peak near K_E. This is especially so if the characteristic wave solution which is neglected has a complex wave number with a small imaginary part so that the resulting attenuation on a short antenna may not be too important. Incidentally, Wunsch (1967) has found the current on a short antenna in a compressible isotropic plasma by solving a pair of coupled integral equations for the current, and finds current components with two different wave numbers on the antenna, one near K_E and the other near K_P.

The four Figs. 6 through 9 which show $i_R(\beta)$ with ν a parameter serve to illustrate the independence of K_{zr} on ν and to verify that the real part of the current wave propagation constant may be obtained as previously outlined. This question will be discussed more in presenting results for K_{zr} in section III b.

TABLE I

Sheathless Case

f=2 MHz, f_p=1.5MHz

T	ν	G	B
^oK	sec^{-1}	millimhos	
1,500	10^4	0.7691	0.1355
1,500	10^2	0.7690	0.1358
1,500	10^1	0.7689	0.1357
1,500	0	0.7679	0.1353
0	10^4	0.7062	0.1556
0	0	0.7061	0.1561
	f=2MHz, f_p=0		
		1.126	0.2663

(b) The Real Wave Number K_{zr}

Having gained some insight into the dependence of $i_R(\beta)$ on the exciting frequency and the plasma parameters, we will now present the results obtained for K_{zr} from the $i_R(\beta)$ variation with β, as shown in the preceding graphs. The K_{zr} values are found, as was previously discussed, from the value of β at which a peak in $i_R(\beta)$ occurs accompanied by a sign change in $i_I(\beta)$. The K_{zr} values thus obtained should be, for a small value of electron collision frequency, nearly the same as the real components of the β_o values which satisfy

$$D(\beta) = 0 \qquad (10)$$

for zero collision frequency, where D is the matrix coefficient determinant previously discussed. Though the K_{zr} values we find by this approach cannot be verified from an analytic solution of (10) for the general case, an approximate solution for the incompressible magnetoplasma as given by (4), and the compressible, isotropic plasma, both for the sheathless case only, can readily be found. The agreement between these approximate analytic solutions for these special cases and the K_{zr} values obtained by the method outlined will be discussed in presenting the results.

We now present in Fig. 10 the real wave number solutions, K_{zr}, as a function of frequency, for the incompressible, anisotropic plasma model for both the sheathless and $5D\ell$ thick vacuum sheath cases. Two sets of curves for each sheath representation are included, one for the case where $f_p = 1.5$ MHz and $f_h = 1.0$ MHz, and the other where the values of f_p and f_h are interchanged. The value of electron collision frequency used here is $\nu = 10^4 \text{sec}^{-1}$, and the antenna radius employed for these calculations is 1 cm.

If we examine first the sheathless cases of Fig. 10, we see that there are no values for K_{zr} between f_h and $f_t (f_t = \sqrt{f_h^2 + f_p^2})$. This result is in agreement with (4) which shows that in this frequency range, the characteristic wave

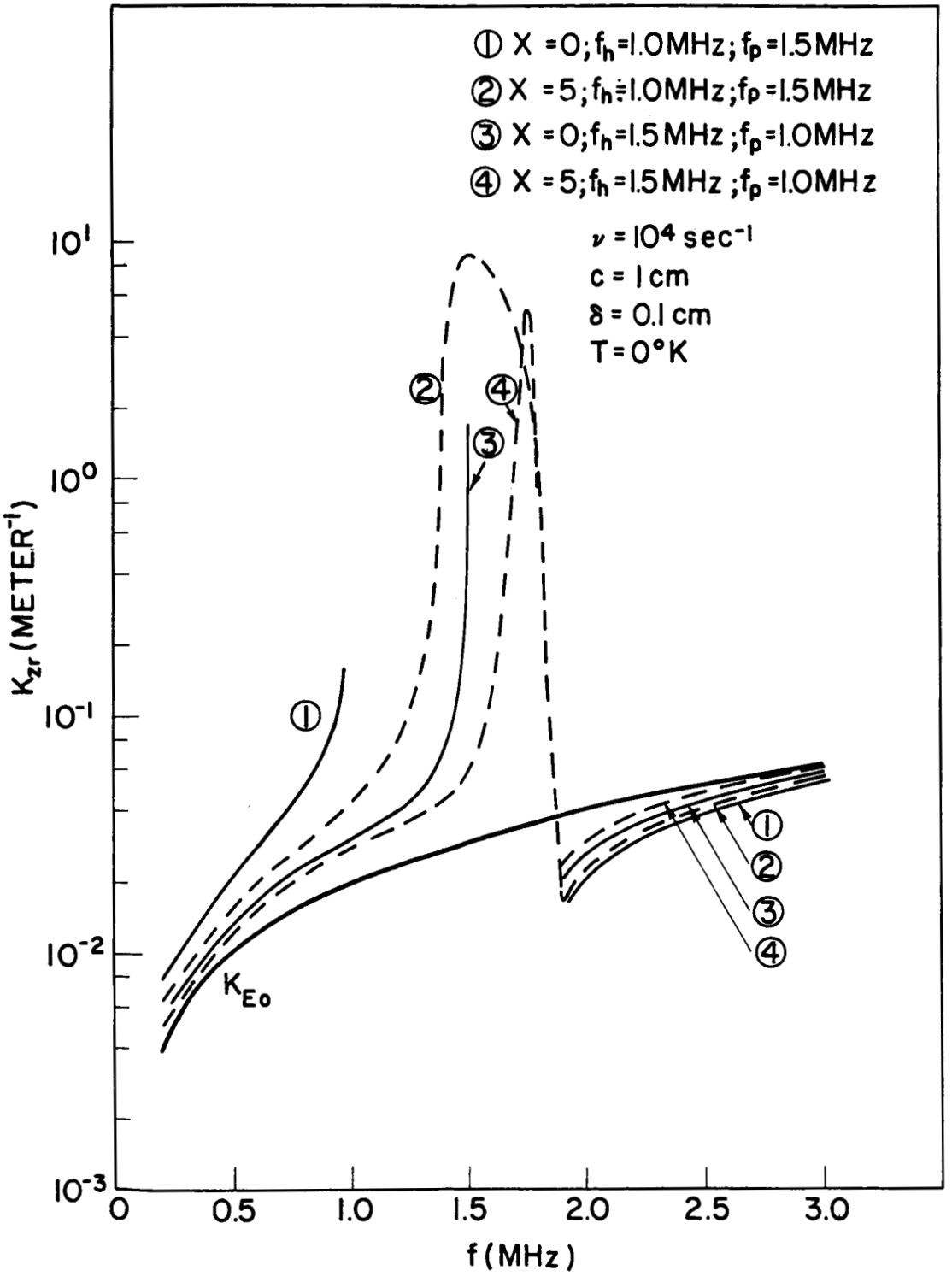

Fig. 10. The real component of the characteristic wave number, K_{zr}, as a function of frequency for the anisotropic, incompressible plasma, and the sheathless and 5 Debye length vacuum sheath cases.

number is pure imaginary and that consequently the current wave is evanescent in the z-direction. The K_{zr} values outside this frequency interval may be verified to be equal to the analytic solution for this case, given by (4).

When the vacuum sheath case is considered however, it is found that there is no cutoff region, but the K_{zr} values become fairly large in the region where the sheathless case is cutoff. The effect of the sheath outside this frequency range is to increase the values of K_{zr} compared with the sheathless case, above f_t, and to decrease them below f_h. When the frequency becomes much larger than f_t or is sufficiently less than f_p and f_h, then K_{zr} may be observed to approach K_{Eo}, the free-space wave number. In the region above f_t, where $K_{zr} \leq K_{Eo}$, the current waves are sometimes called fast waves since their phase velocities exceed the free-space velocity of light, while in the region below f_h and f_t, they may be called slow waves because their phase velocity is less than the velocity of light.

It is of interest to remark that for the sheathless case where an analytic solution may be obtained for K_{zr} as previously mentioned, in the limit of vanishing cylinder radius, the frequency range can be divided into five regions of different wave behavior (see Lee and Lo, 1967). If we denote a surface wave as one which propagates in the z-direction but is evanescent in the radial direction, then the five regions may be characterized as follows: (1) $f > f_t$, one fast wave and one surface wave; (2) $f_p < f < f_h$, one slow wave and one surface wave; (3) $f < f_h$, f_p, two surface waves; (4) f_p, $f_h < f < f_t$, two radially propagating waves evanescent in the z-direction; (5) $f_h < f < f_p$, two waves evanescent in both the z and radial directions. It should be noted that there are two waves because of the birefringence of the medium resulting from its anisotropy, but the two waves have the same magnitude of characteristic wave number.

We next present in Fig. 11 the values for K_{zr} as a function of frequency for both the compressible and incompressible isotropic plasmas, and the sheathless and 5 D_ℓ thick vacuum sheath cases. The plasma frequency is 1.5 MHz and the other parameter values are the same as used for Fig. 10. It is very interesting to see that above f_p, there are two characteristic wave number solutions, one which is approaching K_{Eo} with increasing frequency, and the other which is approaching K_{Po}, where

$$K_{Po} = \frac{\omega}{v_r}$$

with v_r the rms electron velocity. The existence of two characteristic waves is significant, and results from the plasma compressibility, the one whose wave number is near K_{Eo} being an electromagnetic type wave and the other being an acoustical or electrokinetic wave. The relative importance of the two waves in determining the antenna admittance depends very much on the contribution to the total current resulting from the currents associated with the characteristic waves, a topic which has been previously discussed, and which will be pursued further in the next section.

Below the plasma frequency, we observe that there is no wave number solution for the sheathless, incompressible plasma, a result which is in agreement with the formula given by (4) if H is set equal to zero there. The other three cases shown on Fig. 11 do however have solutions below f_p, which may be seen to peak rather sharply near f_p where they approach K_{Po}, then decreasing in value with decreasing frequency so that sufficiently below f_p, they again approach K_{Eo}. This behavior is similar to that found for the case of the incompressible, anisotropic plasma shown in Fig. 10.

While an approximate analytic solution has been presented above for K_{zr} for the incompressible magnetoplasma, we have not discussed this possibility for the compressible, isotropic plasma. The development of

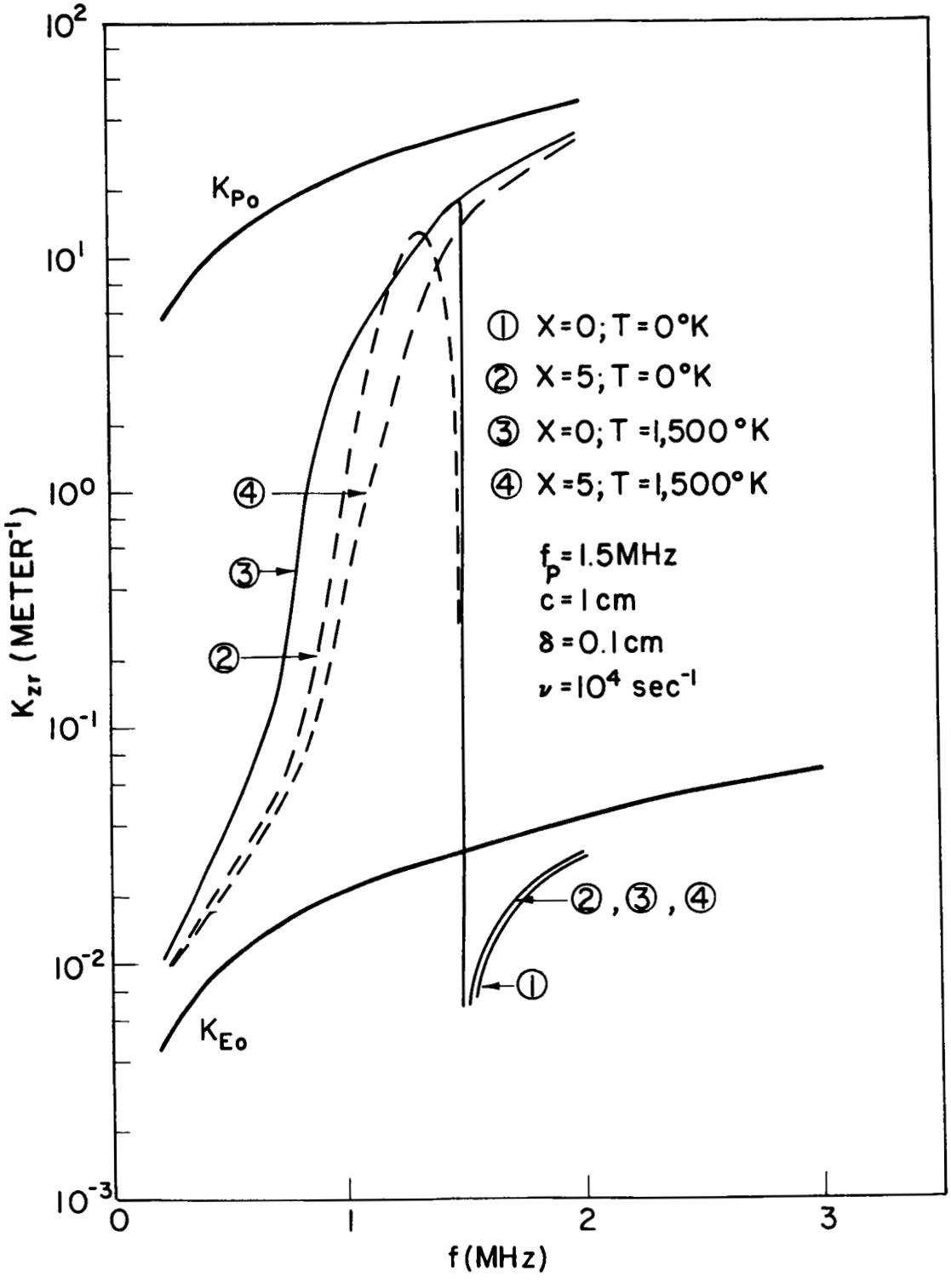

Fig. 11. The real component of the characteristic wave number, K_{zr}, as a function of frequency for the isotropic incompressible and compressible plasmas, and the sheathless and 5 Debye length vacuum sheath cases.

Appendix C includes a discussion of this, where from the small argument approximations for the cylindrical functions it is shown that above f_p, two possible solutions for K_{zr} are given by

$$K_{zr}^2 = \mathrm{Re}\beta_o^2 = \frac{K_{Eo}^2(1-N^2)}{1 - \dfrac{N^2 \ln(\lambda_P c\,\Gamma/2)}{\ln(\lambda_e c\,\Gamma/2)}} \quad ; \quad \beta < K_{Eo} \tag{9}$$

and

$$K_{zr}^2 = \beta_o^2 = K_{Po}^2(1-N^2) \tag{10}$$

where

$$\lambda_P = \sqrt{K_{Po}^2(1-N^2) - \beta^2}$$

$$\lambda_e = \sqrt{\beta^2 - K_{Eo}^2(1-N^2)}$$

and the electron collision frequency is taken to be zero. The first expression above, (9), is seen to be transcendental, involving β on both sides of the equation. Since a solution for β will be on the order of K_{Eo}, the log term in λ_P will have an argument on the order of v_r/v_ℓ times that of the log term in λ_e. Because the log arguments are smaller than unity, then the ratio of the log terms will be less than unity and the denominator of (9) will be larger than $1-N^2$. Consequently the solution for β should be less than K_{Eo}, but not as small as that found for the incompressible plasma, $K_{Eo}\sqrt{1-N^2}$, which is indeed the case as shown on Fig. 11. The solution for β near K_{Po} given by (10) is also found to agreement with the calculated results of Fig. 11.

When $f < f_p$, only one solution is obtained, and it is given by (9) also, but with λ_P replaced by

$$\lambda_p = \sqrt{\beta^2 - K_{Po}^2(1-N^2)} = -i\lambda_P$$

If N becomes large enough, then (9) is approximately

$$K_{zr}^2 = \beta_o^2 \quad \frac{K_{Eo}^2 \ln(\lambda_e c \Gamma/2)}{\ln(\lambda_p c \Gamma/2)} \tag{11}$$

Again, since $\lambda_p > \lambda_e$, and the log arguments are less than unity, their ratio in (11) is larger than unity, and β exceeds K_{Eo}, as shown by the graphs of Fig. 11. In the range where N is near unity, then an approximate solution for β is

$$\beta^2 \approx (N^2-1)^{N^2} K_{Po}^{N^2} \left(\frac{c\Gamma}{2}\right)^{N^2-1} \tag{12}$$

This expression may be verified by calculation to be also in approximate agreement with the results of Fig. 11.

It is interesting to observe that the characteristic wave solution below, but near, the plasma frequency, is a hybrid wave involving both the electron thermal motion and the electromagnetic type wave. This solution does not exist when the plasma is incompressible, as may be verified in Appendix C where the limit $v_r \longrightarrow 0$ is investigated. It may also be verified that (9) and (10) may be combined into one expression, as

$$K_{zr}^2 = \beta^2 = \frac{K_{Eo}^2(1-N^2)}{1 - \dfrac{\ln(|\lambda_p| c \Gamma/2)}{\ln(|\lambda_e| c \Gamma/2)} N^2} \tag{13}$$

which is valid for any $f \neq f_p$.

The K_{zr} values for the compressible magnetoplasma, and the sheathless case only, are shown in Fig. 12, where an electron temperature of $1,500^{\circ}K$ has been used together with the plasma and cyclotron frequency values employed for the incompressible magnetoplasma results of Fig. 9. The collision frequency is again $10^4 sec^{-1}$. The results shown here for the compressible magnetoplasma are very similar to the corresponding curves

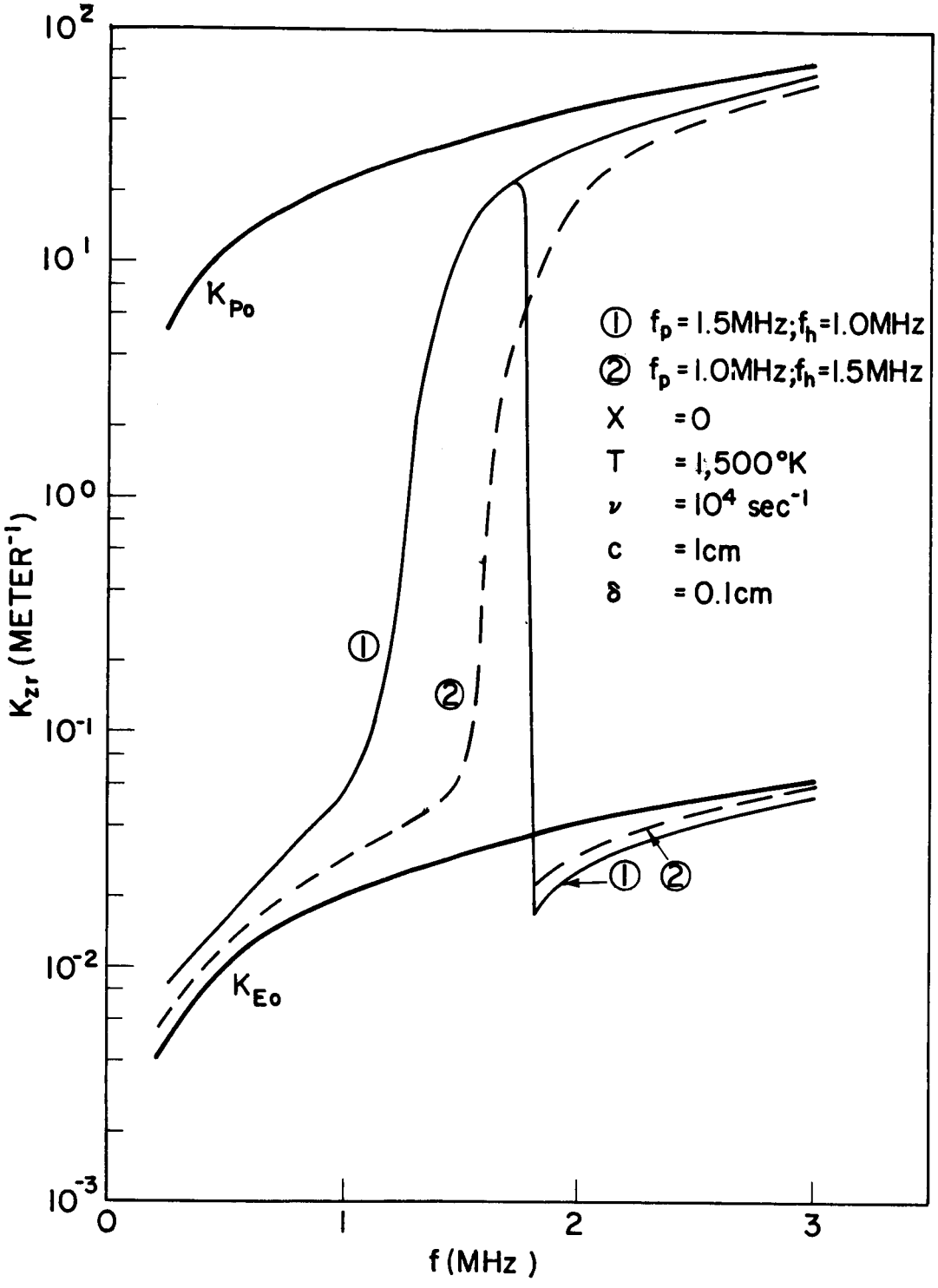

Fig. 12. The real component of the characteristic wave number, K_{zr}, as a function of frequency for the anistropic compressible plasma and the sheathless case only.

of Fig. 9 for the incompressible magnetoplasma, below the upper hybrid frequency. Above f_t however, are found two characteristic wave number solutions, one near K_E and the other near K_P. We again see evidence of the plasma compressibility then through a characteristic wave number which is dependent upon the thermal electron velocity in the plasma. The current contribution coming from the peak near K_P is found to be of little importance compared with that due to the peak near K_E however, a result similar to that found for the isotropic compressible plasma.

(c) The Antenna Peak-to-total-Real-Current Ratio.

The ratio of the real antenna current at the exciting gap coming from the integration range $\beta = 0.9K_{zr}$ to $\beta = 1.1K_{zr}$ to the total real gap current is shown in the next set of graphs, which are presented in the same order as in the previous section. It should first be mentioned however, that while the compressible plasma model was found to have two wave number solutions above f_p or f_t, depending on whether the plasma is isotropic or anisotropic, the current contribution coming from the wave number near K_P amounted to less than 10^{-4} of the total current. Consequently, on the current ratio curves to be shown, we restrict our attention to the wave number near K_E, above f_p or f_t. Below these frequencies there is only one solution for K_{zr}, which is the one used in obtaining the current ratios to be given.

In Fig. 13 are shown the current ratios as a function of frequency for the incompressible magnetoplasma for the same sets of plasma parameter values as employed for Fig. 10. We note that above f_t and below f_h the ratios are generally 0.5 or larger. While the sheathless cases are not shown between f_t and f_h because there are no K_{zr} solutions there, the vacuum sheath curves do cover the entire frequency range considered. It may be seen that the vacuum sheath current ratios are smaller than 0.1 in the frequency range extending roughly from f_t down to $(f_t+f_h)/2$. It is obvious that the width of the frequency

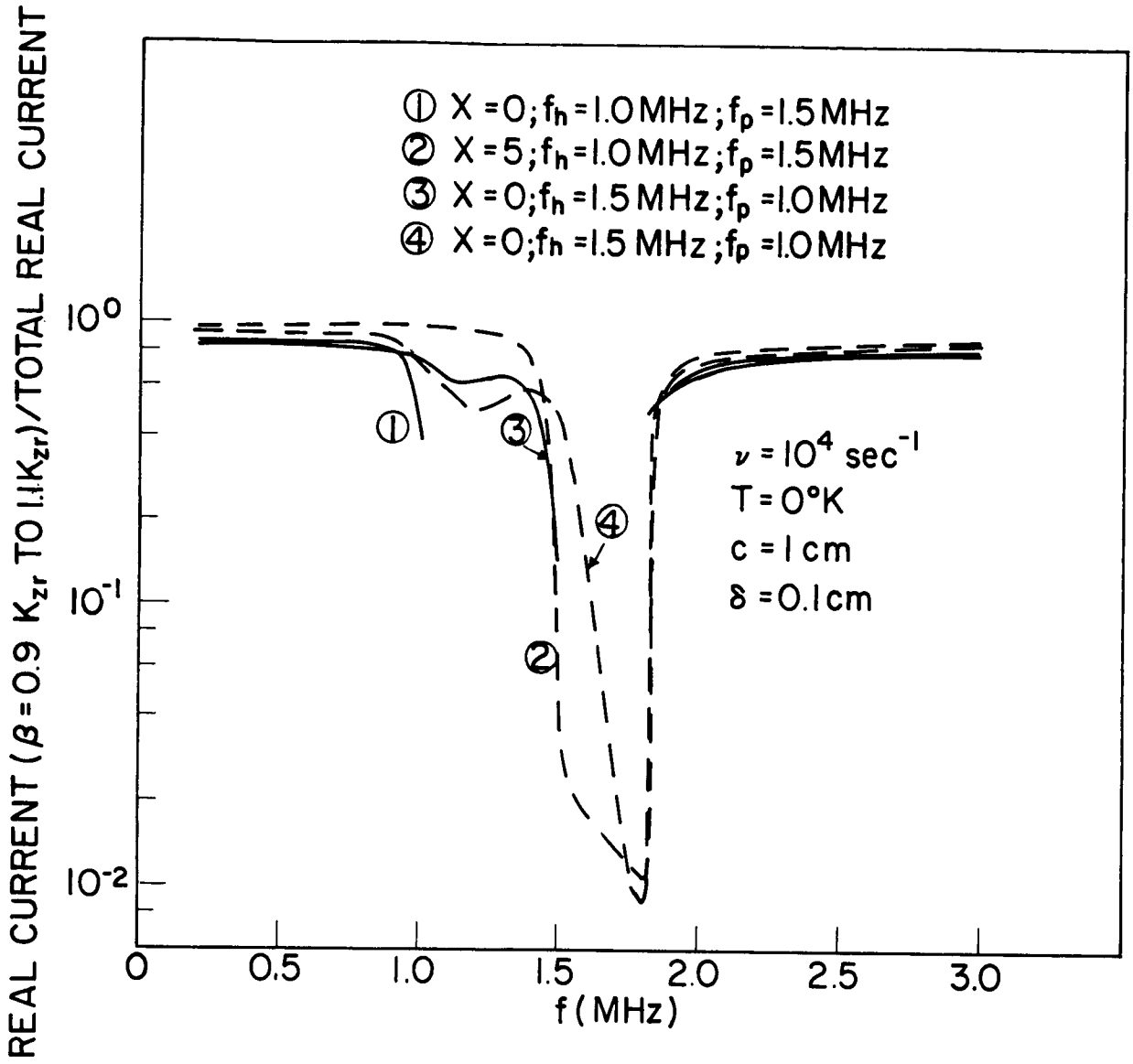

Fig. 13. The real current ratio (real current from β = 0.9K_{zr} to 1.1 K_{zr} to total real current) as a function of frequency for the anisotropic, incompressible plasma and the sheathless and 5 Debye length vacuum sheath cases.

range of small current ratios is dependent upon the vacuum sheath thickness, the thicker the sheath the narrower the resulting frequency interval of small current ratios.

We may thus conclude that in any case, above f_t and below f_h, the antenna current will have a wave-like behavior with a wave number given by K_{zr}. When there is a vacuum sheath present, the wave-like behavior will extend to frequencies somewhat higher than f_h. There is a cutoff region between f_t and the vicinity of f_h where there is no appreciable propagating current wave along the antenna, which is in agreement with the analysis of Lee and Lo (1967) outlined above, and where the current decays in the z-direction.

The current ratios for the isotropic compressible and incompressible plasmas and the sheathless and vacuum sheath cases corresponding to the results of Fig. 11 are shown in Fig. 14. It may be seen that above f_p, all the ratios are on the order of 0.5 or larger. Below approximately 1.4 MHz, with the exception of the sheathless, incompressible case which has no K_{zr} solution below f_p, the current ratios are again 0.5 or larger. The antenna current is thus expected to have a wave-like behavior with wave number K_{zr} at all frequencies except in the immediate vicinity of f_p for the compressible and/or sheathed isotropic plasma.

The last graph of this section, Fig. 15, shows the current ratios for the sheathless, compressible, anisotropic plasma for the plasma parameter values used in Fig. 12. Here it may be seen that the current ratios are larger than 0.5 above 2 to 2.5 MHz and below 1.5 MHz, with the current ratio for $f_h = 1.5$ MHz exceeding that for $f_h = 1.0$ MHz over most of the frequency range. A comparison of Fig. 15 with the vacuum sheath curves of Fig. 13 shows them to be very similar. A similar observation can be made about the K_{zr} curves of Figs. 10 and 12. It is interesting to note that the corresponding admittance

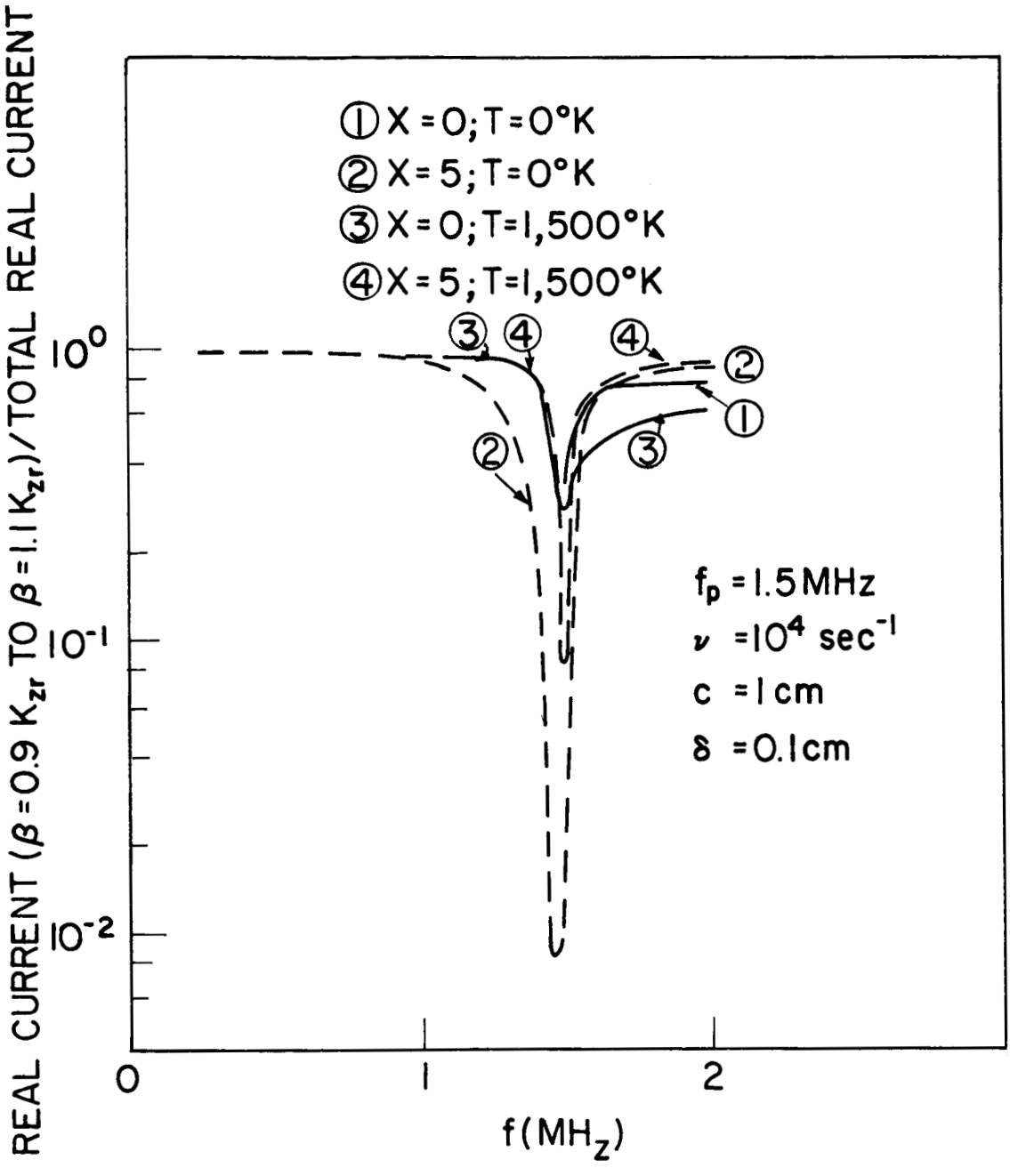

Fig. 14. The real current ratio (real current from β = 0.9K_{zr} to 1.1 K_{zr} to total real current) as a function of frequency for the isotropic compressible and incompressible plasmas, and the sheathless and 5 Debye length vacuum sheath cases.

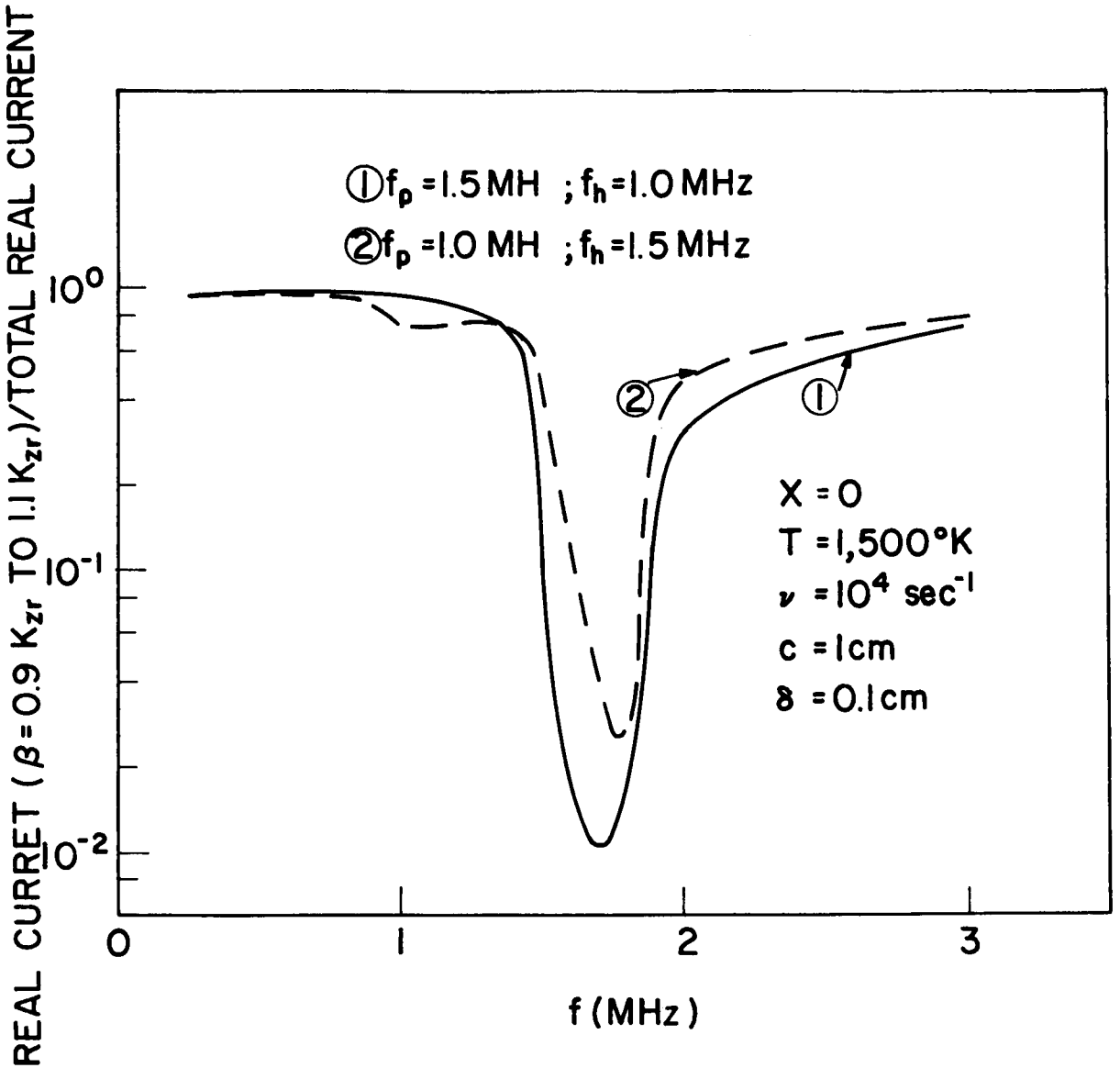

Fig. 15. The real current ratio (real current from $\beta = 0.9K_{zr}$ to $1.1 K_{zr}$ to total real current) as a function of frequency for the anisotropic compressible plasma and the sheathless case only.

results for these two cases are also quite similar, reflecting the interrelationship which exists among these quantities, and the similarity of the vacuum sheath and plasma compressibility influence on the infinite antenna. This observation also holds for the isotropic plasma.

(d) Antenna current as a function of z.

A limited amount of results for the axial current on the antenna obtained from a direct evaluation of the Fourier integral for the antenna current are presented in this section. As in section (a), the discussion here is for the isotropic plasma only, since the nature of the results and the conclusions that can be drawn from them are not necessarily dependent on the plasma model used.

The total complex antenna current ($2\pi c$ times the surface current/unit length) is shown as a function of z in Fig. 16 for the incompressible plasma with a $5D_\ell$ vacuum sheath, a frequency of 1.55 MHz, and the other plasma parameter values as used for the preceding isotropic plasma results. We see that the real current component, shown by a solid line, varies in a more regular way with increasing z than does the imaginary component, shown by a dashed line. The wave-length of the current sample shown on Fig. 16 is for the real component about 680 m, corresponding to a wave number of $9.24 \times 10^{-3} m^{-1}$. The value of K_{zr} on Fig. 11 for this particular case is $9.5 \times 10^{-3} m^{-1}$. This result, together with the current ratio graph for this case as shown on Fig. 14, demonstrates the validity of the method used for finding the characteristic wave solutions as previously outlined and determining the wavelike nature of the antenna current.

It is apparent that the imaginary part of the axial antenna current has some higher spatial frequency components than does the real current, as evidenced by the oscillations superimposed on the predominant wave behavior

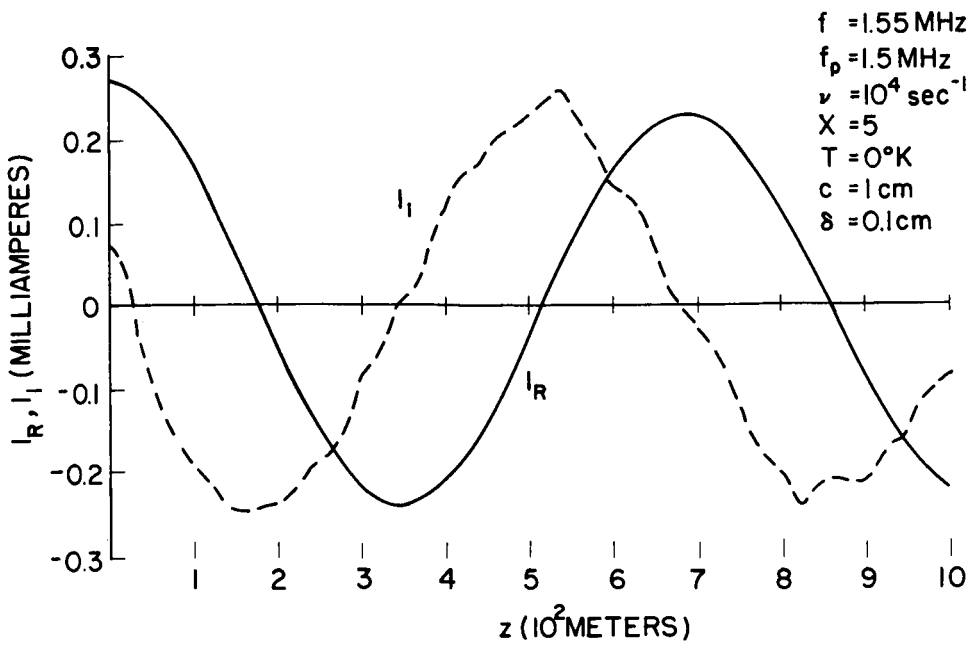

Fig. 16. The real and imaginary components of the infinite antenna current as a function of axial distance z from the exciting gap for the isotropic incompressible plasma and $f > f_p$ with a 5 Debye length vacuum sheath.

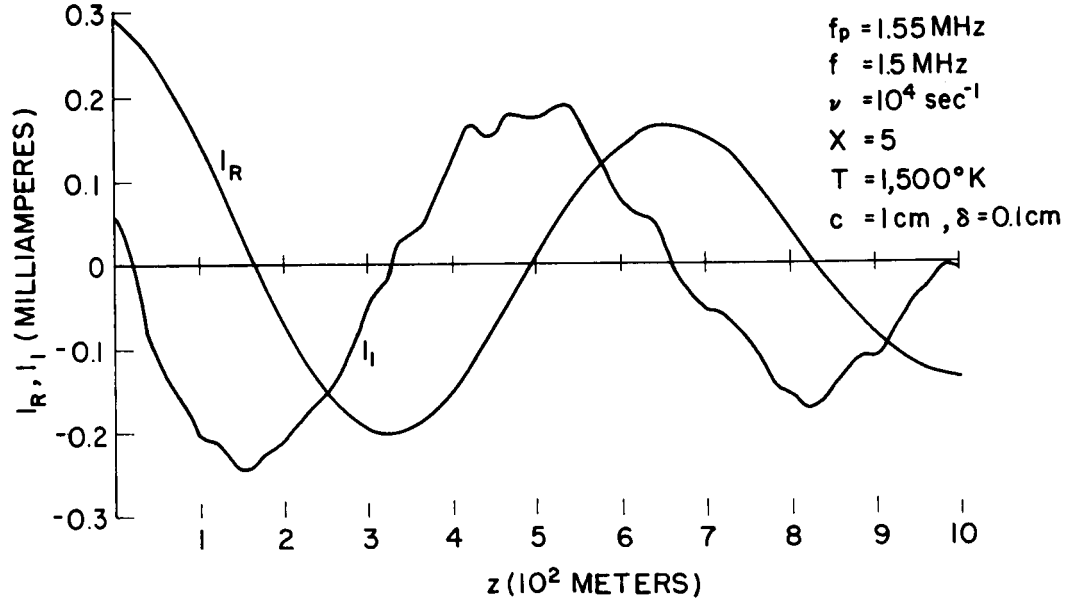

Fig. 17. The real and imaginary components of the infinite antenna current as a function of axial distance z from the exciting gap for the isotropic compressible plasma and $f > f_p$ with a 5 Debye length vacuum sheath.

which varies as K_{zr}. Since the integration range required to find the imaginary current extends to larger values of β than does the corresponding integration range for the real current (this is discussed more fully in I) this is not unexpected. Taking both current components together however, as plotted in Fig. 15, the surface current on the antenna varies nearly as $\exp\left[i(\omega t - K_{zr}z)\right]$. A(z), where A(z) is an attenuation factor.

The case of the compressible, $5D_{\ell}$ vacuum sheath model is shown next in Fig. 17, again for a frequency of 1.55MHz and the other plasma parameter values as used for Fig. 16. The results shown on Fig. 17 are similar to those of Fig. 16 for the incompressible case except that the antenna current in the latter case exhibits somewhat more superimposed ripple. The current wave length in Fig. 17 from the real component is approximately 640 m, so that the wave number is $9.82\times10^{-3}m^{-1}$, which is again in agreement with the graph of Fig. 11.

The current of Fig. 17 may also be approximately represented by $\exp\left[i(\omega t - K_{zr}z)\right]$. A(z) where now the function A(z) appears to be a more rapidly decreasing function of increasing z than was the case for the incompressible plasma. This attenuation of the current with z may be greater for the compressible plasma as compared with the incompressible plasma because the EK wave experiences more loss per unit length in the lossy plasma due to its shorter wave length. Viewed in another way, the spatial frequency spectrum of the transformed current is broader and less peaked for the compressible plasma than for the incompressible plasma, which produces the increased z-attenuation of the current for the former case. This is illustrated by the $i_R(\beta)$ curves shown in Figs. 1 and 2. A greater z-attenuation may also be indicated by a smaller current ratio which is also an indication of an increased dispersion of spatial frequency content in the $i_R(\beta)$ curve. Finally, we have pointed out

that the characteristic wave solution near K_E is complex, for the compressible plasma, thus indicating an attenuation in the z-direction of the total current which comes principally from the current peak associated with the characteristic wave number solution near K_E.

In order to further demonstrate the feasibility of determining the general nature of the antenna current from the K_{zr} solutions and the current ratios or the $i_R(\beta)$ curves we present in Figs. 18 and 19 respectively the complex antenna currents for the incompressible and compressible plasmas and the $5D_\ell$ vacuum sheath, for frequencies of 1.45 and 1.50 MHz, the other parameter values remaining the same as for Figs. 16 and 17.

We see that at 1.45 MHz, which is less than the plasma frequency of 1.5 MHz, the currents for both the compressible and incompressible plasmas decay quite abruptly near the exciting gap, with the real component in particular becoming negligible at distances greater than 100 m from the source. The imaginary component, after the initial fall-off, is oscillatory in nature, but exhibits no clear wavelength, as do the currents at f=1.55MHz. It should be mentioned here that the current was calculated at 20m intervals, so that a current wavelength shorter than this would not be detected. However, because of the problems previously discussed concerning the field and current calculation when the sequence of abscissa values is determined only by the admittance evaluation, it does not appear worthwhile to find the current at a closer spacing along the antenna axis since the accuracy cannot be expected to be very good beyond 100 to 200m. The results should provide a reasonable order of magnitude for the current however, especially for the real component whose effective integration range is much less than for the imaginary component, as mentioned above.

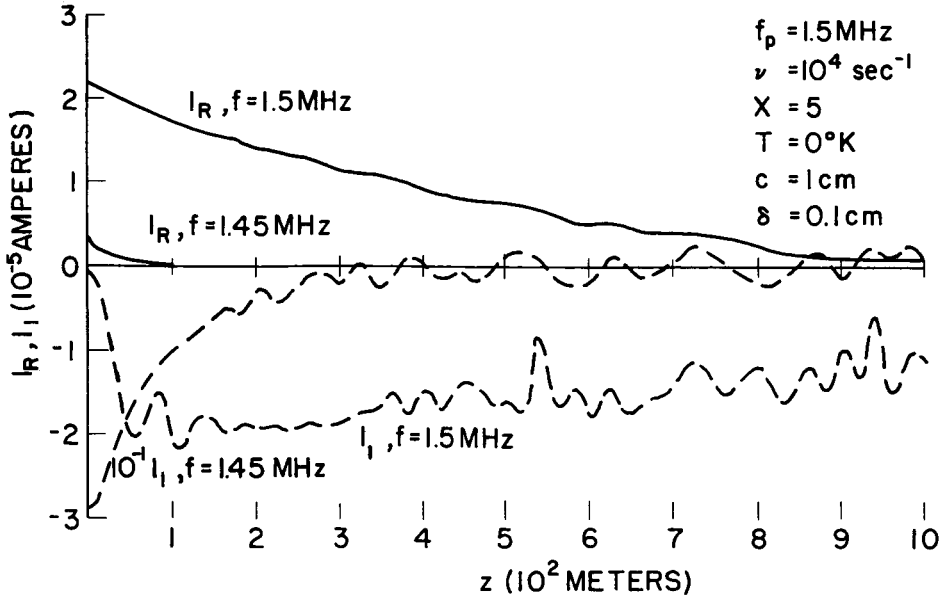

Fig. 18. The real and imaginary components of the infinite antenna current as a function of axial distance z from the exciting gap for the isotropic incompressible plasma and the two cases $f < f_p$ and $f = f_p$, with a 5 Debye length vacuum sheath.

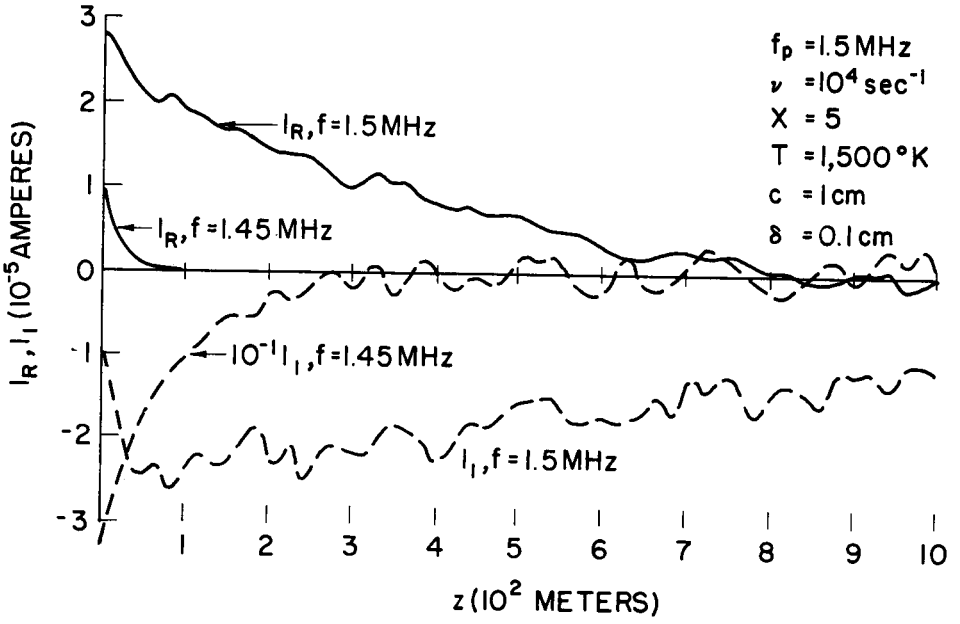

Fig. 19. The real and imaginary components of the infinite antenna current as a function of axial distance z from the exciting gap for the isotropic, compressible plasma and the two cases $f < f_p$ and $f = f_p$, with a 5 Debye length vacuum sheath.

The currents at 1.5 MHz do not decay as rapidly as is found at 1.45 MHz. The imaginary component as a matter of fact, actually increases rather abruptly upon moving away from the exciting gap. The real current component for the compressible plasma is again seen to be more oscillatory than that for the incompressible case, a result similar to that previously remarked on for f = 1.55 MHz. The axial current curves plotted on Figs. 16 through 19 show that when the current ratio is small as at 1.45 and 1.50 MHz, the antenna current may be oscillatory, but not generally wavelike in nature. When however, the ratio is near unity, as at 1.55 MHz, the current does vary along the axis with a predictable wavelength that corresponds well with K_{zr}.

(e) The Antenna Near Fields.

The fields near the antenna were calculated for the isotropic plasma and the $5D_{\ell}$ vacuum sheath only, for both the compressible and incompressible plasmas. The plasma parameter values used were the same as employed for the isotropic plasma results thusfar presented and the frequencies used for the calculation were 1.45, 1.5 and 1.55MHz, so that the plasma frequency of 1.5MHz could be bracketed. The complex components of the z and ρ electric fields, of both the EM and EK modes, the ϕ component of the magnetic field and the perturbed electron number density were calculated for the compressible plasma, while only the EM field quantities were of course to be obtained for the incompressible plasma.

Because of the number of field quantities involved, and the fact that the fields are dependent upon both ρ and z, it is not practical to present a detailed graphical picture of the variation of each field quantity with z and ρ. Instead, we have chosen to present here only a limited amouth of the field calculation results which are felt to provide a typical picture of the significant aspects of the infinite antenna near field behavior. In addition, since the

surface current results of the previous section show a z-dependence which is characteristic of that of the other field quantities, we will give results here for only the ρ-variation of the fields.

In Fig. 20 is shown the **magnitude** of the z-component of electric field as a function of ρ at z=0 for the incompressible plasma, and the $5D_{\ell}$ vacuum sheath and for the three frequencies specified above. It is immediately evident from the graph that the ρ-dependence of the z-directed electric field is not very sensitive to the exciting frequency, particularly when note is made of the fact that the frequencies used encompass the electron plasma frequency.

Also of interest in this regard is the fact that the rate of decrease of the electric field with increasing radius is approximately ρ^{-1} for the larger radii. This rate of decrease may at first thought be somewhat surprising since the fields due to a source in a cylindrical geometry are known to decrease as $\rho^{-1/2}$. However, while a cylindrical structure is involved here, the source is of finite dimension, being the voltage applied across the exciting gap at z=0 so that an inverse ρ dependence is required for large ρ. If, of course, the source were to extend to infinity along the antenna surface (i.e. an axial rather than a circumferential gap), a $\rho^{-1/2}$ dependence would be produced. The slight excess of the field decrease over a ρ^{-1} dependence as shown on Fig. 20 is due to the lossyness of the plasma medium.

The z-component of the electric field is shown on Figs. 21 and 22 for the compressible plasma, again for the $5D_{\ell}$ vacuum sheath and the three frequencies employed in Fig. 20, with Fig. 21 showing the EM electric field and Fig. 22 the EK electric field. Also shown on Fig. 21 is the magnitude of the total z-component of electric field obtained by adding the separate complex amplitudes of the EM and EK components.

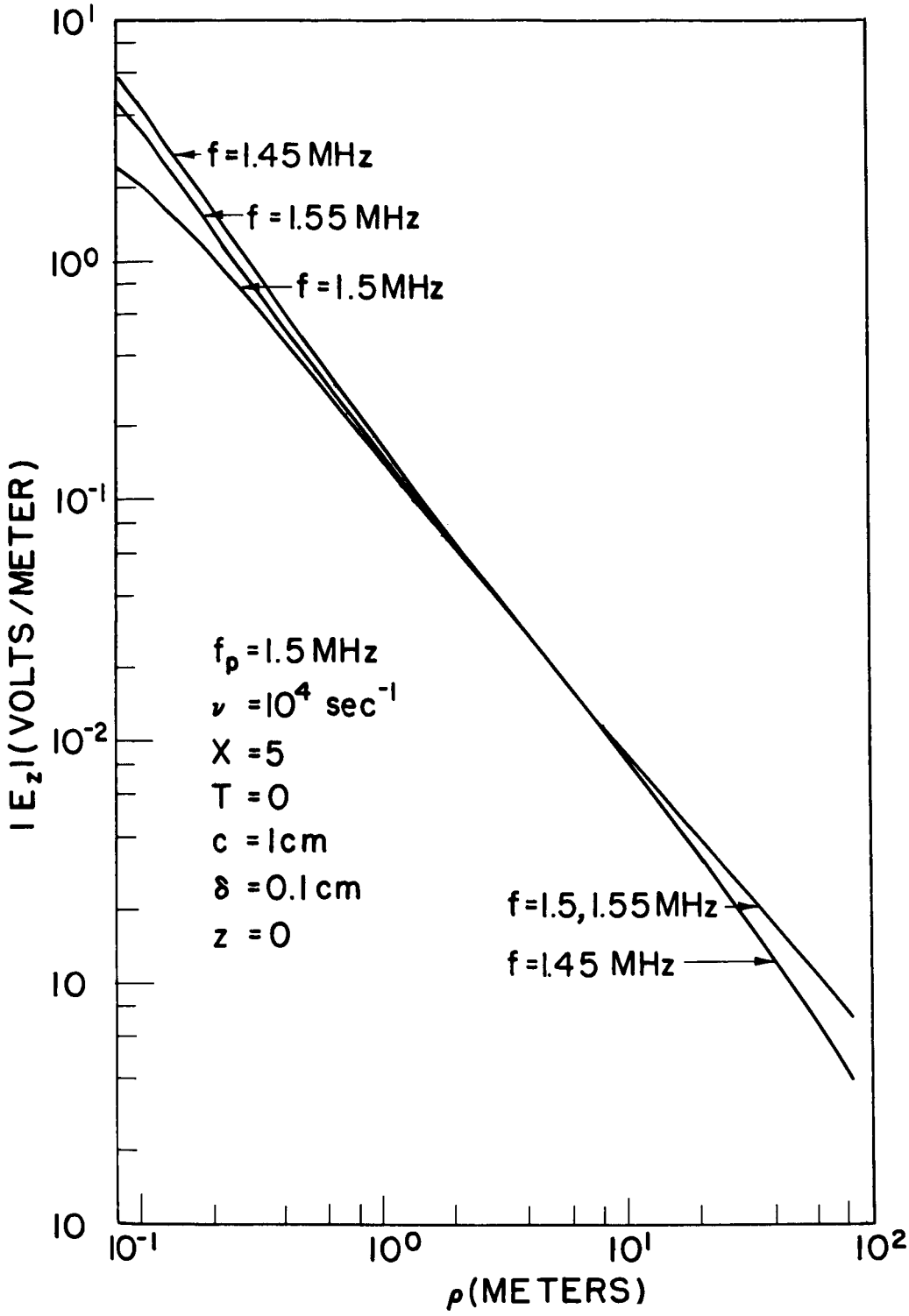

Fig. 20. The magnitude of the z-component of electric field at z = 0 as a function of ρ (s=0.0899m) for frequencies f less than, equal to, and greater than f_p and the isotropic, incompressible plasma and 5 Debye length vacuum sheath.

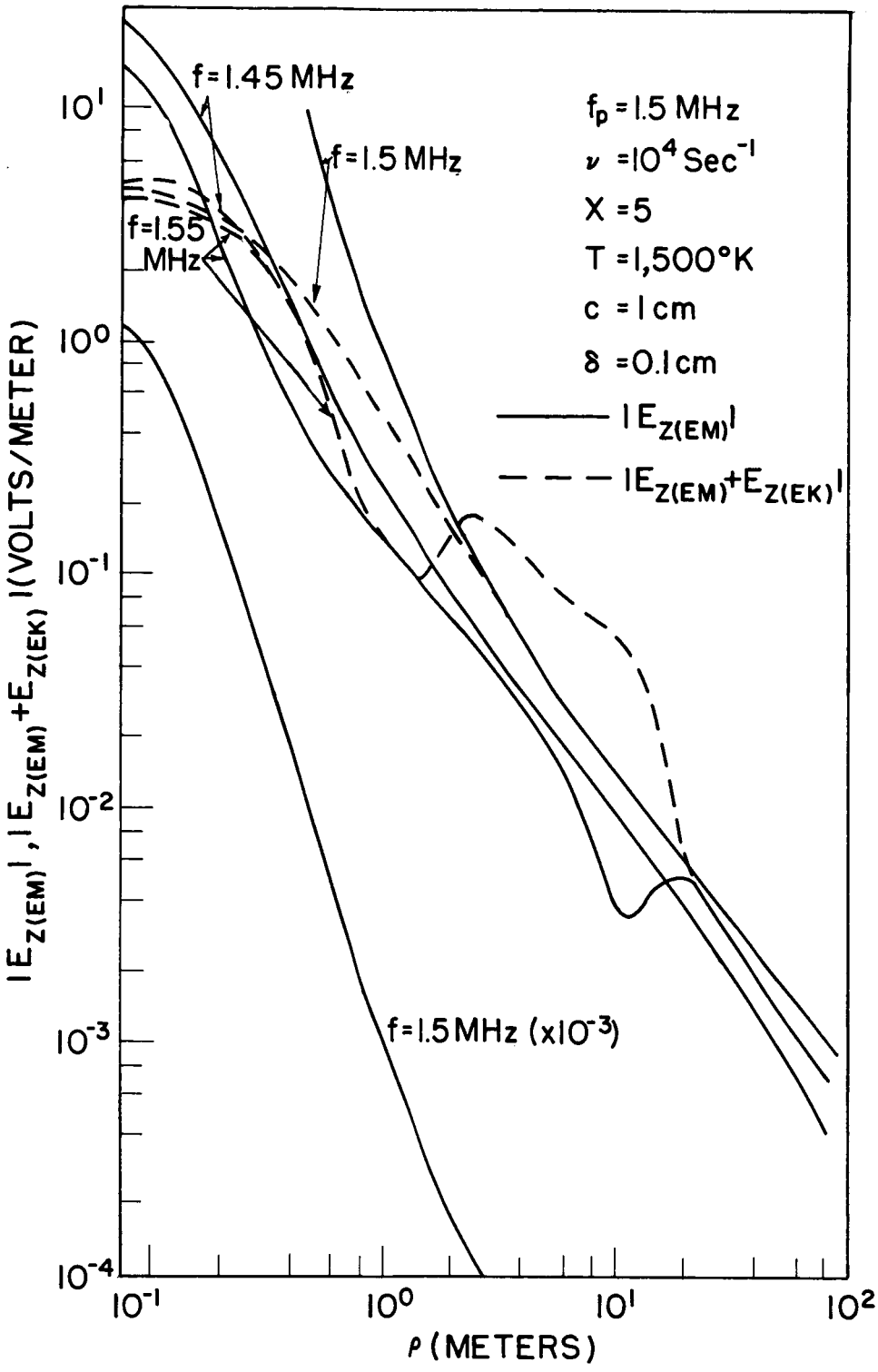

Fig. 21. The magnitude of the z-component of the EM electric field, $|E_{z(EM)}|$, and the total electric field, $|E_{z(EM)} + E_{z(EK)}|$ at z = 0 as a function of ρ (s=0.0899m) for frequencies f less than, equal to, and greater than f_p and the isotropic compressible plasma and 5 Debye length vacuum sheath.

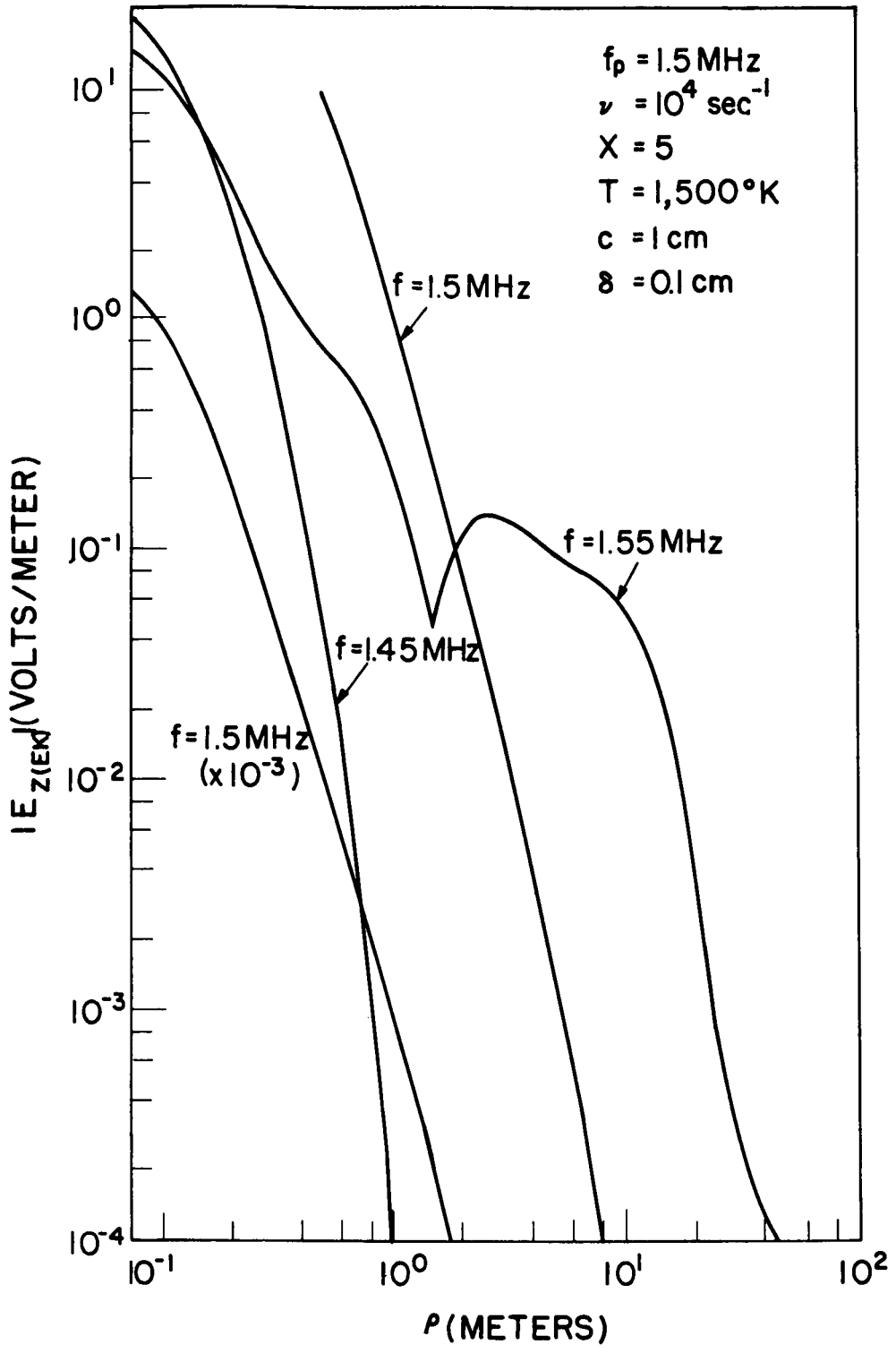

Fig. 22. The magnitude of the z-component of the EK electric field $|E_{z(EK)}|$ at z = 0 as a function of ρ (s=0.0899m) for the frequencies f less than, equal to, and greater than f_p and the isotropic compressible plasma and 5 Debye length vacuum sheath.

A comparison of Fig. 21 with the corresponding curves of Fig. 20 shows that for the compressible plasma the EM electric field is, at 1.45 and 1.55 MHz, similar to that obtained for the incompressible plasma, the major difference being that for the compressible case the field magnitude at the sheath edge is somewhat higher, and the field decrease with increasing ρ exhibits a more oscillatory behavior. At 1.5 MHz however, the compressible plasma EM electric field is seen to be almost three orders of magnitude larger at the sheath edge than is the incompressible value, but falls off so rapidly with increasing ρ that at about 5 to 10 m, the incompressible and compressible values are nearly equal.

The EK electric field magnitudes shown in Fig. 22 may be seen to have values at the sheath edge nearly the same as the EM fields of Fig. 21. As for the EM fields, the EK electric field at 1.5 MHz is about two orders of magnitude larger than the values at 1.45 and 1.55 MHz. The EK electric field is seen to decrease with ρ more rapidly than the EM fields, particularly at 1.45 and 1.50 MHz, reflecting the fact that the radial propagation constant of the EK wave is larger than that of the EM wave by the ratio v_{ℓ}/v_r.

The most significant feature exhibited by Figs. 21 and 22 is the fact that the total z-directed electric field at 1.5MHz, obtained as the complex sum of the EM and EK components is, as shown on Fig. 21, almost three orders of magnitude less than the individual components, and on the same order as the EM field for the incompressible case shown in Fig. 20. The EM and EK fields which individually become large at 1.5MHz compared with those at 1.45 and 1.55MHz, are at the same time nearly 180° out of phase thus effectively cancelling out their increased magnitudes. Some cancellation also takes place at 1.45 and 1.55MHz, but not to the same extent, as shown by the total field curves for these frequencies also shown on Fig. 21.

This near equality in magnitude, and phase opposition of the z-directed EM and EK electric fields also occurs for the ρ-directed electric fields. It arises because of the boundary condition used for the electron velocity at the sheath-plasma interface in this study. The boundary condition used here is that the electrons which impinge on the sheath-plasma interface are elastically reflected there, a type of boundary commonly called the rigid or hard boundary. Since, at the plasma frequency, the EM and EK components of the electron velocity are proportional, with nearly the same proportionality constants, to their respective electric fields (to within a factor on the order of $1+i\nu/\omega$), the cancellation of the EM and EK electron velocity components due to the hard boundary condition also results in the near cancellation of their electric fields.

While the total electric field is understandably much smaller than the component EM and EK electric fields at the plasma frequency, the increase in magnitude of these components in comparison with their values just below and just above the plasma frequency is somewhat surprising. This is especially so since the EM electric field in the incompressible plasma does not exhibit this type of behavior. It appears however that the antenna excites pretty much the same total electric field value in either the compressible or incompressible plasma, and because of the field cancellation due to the velocity boundary condition at the plasma frequency, the individual EM and EK fields must be that much larger in the compressible plasma to produce the total electric field value required.

This peaking of the EM and EK electric fields at the plasma frequency in the compressible plasma may bear some relationship to the relaxation resonance that has been observed using rocket or satellite-borne antennas in the ionosphere. The relaxation resonance is seen as a ringing of the plasma at characteristic frequencies such as the electron plasma and cyclotron frequencies after turning off the exciting signal. Fejer and Calvert (1964) have suggested

that the relaxation resonance may be due to a matching of the antenna velocity and the electrostatic (EK) oscillation group velocity, which is minimized at f_p, so that the antenna remains in a region of high electric field for a relatively long time. The results obtained here would tend to support this contention to some extent, but provide additional insight into the problem. Since the group velocities of the EM and EK waves are in the ratio of the velocity of light in free space to the rms electron velocity, the EM fields would propagate away from the antenna more rapidly than the EK fields. Consequently, the EM and EK electric field cancellation at the plasma frequency would not persist indefinitely after removing the exciting signal from the antenna, with the result that the total electric field near the antenna may appreciably increase in value before finally falling to zero as the antenna moves out of the field of the EK wave.

Thus, in addition to the effect of the small EK group velocity near the plasma frequency producing a slowly decaying electric field near the antenna to account for the relaxation resonance, we have the increased magnitudes of the component EM and EK fields at the plasma frequency and their large difference in group velocity to also account for the relaxation resonance. In other words, the resonance may be due to both the increased field magnitudes and decreased group velocities which result at the plasma frequency. It must be remarked that the large EM and EK electric fields at f_p result from the hard boundary condition, about the validity of which there is some justifiable skepticism. In addition our discussion here of the fields has been confined to the isotropic plasma, while the ionospheric plasma is of course anisotropic, a factor which may be expected to somewhat modify the findings given for the fields. The extension of the field calculations to the compressible magnetoplasma may thus be indicated, though this is a very much more complicated situation than the case considered, and there is no guarantee that the

calculations may be readily performed to the required accuracy. When the plasma frequency sufficiently exceeds the electron cyclotron frequency however, the plasma is nearly isotropic and the results presented here may be quite close to the situation of interest in the ionosphere.

IV. Discussion

One of the motivations for the present study of the infinite antenna immersed in a plasma medium has been the fact that a finite antenna may be regarded as a truncated, infinite system. Thus, by investigating the current waves which propagate on the infinite antenna and assuming that the finite antenna current consists of multiply reflected current waves of the type propagating on the infinite antenna, the finite antenna current, and its admittance, may be studied. One advantage of this is that the formulation of the infinite antenna problem may be carried out using a rigorous boundary value problem approach, and that the infinite antenna current is obtained from a Fourier integral, rather than as a solution to an integral equation as may be the case for the finite antenna. This is particularly important in a problem involving a compressible plasma medium, since then a pair of coupled integral equations arise whose solutions yield the finite antenna current.

Thus as a first step in examining the finite antenna in a complex environment such as a compressible magnetoplasma, it appears very worthwhile to look at the infinite antenna problem. In addition, the medium influence on the finite and infinite antennas may be suspected to be similar to some extent (this is shown in the results of I and II for the incompressible isotropic and anisotropic plasmas), so that the infinite antenna admittances may produce some insight into the behavior of the finite antenna in the same plasma medium.

Among the more interesting findings of this study has been the fact that above the plasma frequency, or the upper hybrid frequency for the magnetoplasma, the plasma compressibility has little effect on the infinite antenna admittance. This result may be a little unexpected when compared with some previous studies of antenna admittance in a compressible plasma (see Cohen, 1962; Chen, 1964; Cook and Edgar, 1966).

where it was found that the EK wave may play a dominant role in establishing the antenna admittance. It becomes more understandable when the $i_R(\beta)$ curves are examined, where it is found that the compressibility does indeed affect the shape of the transformed current as a function of β, but in such a way as to have little effect on the value of the Fourier integral for the admittance.

The plasma compressibility also gives rise to a second characteristic wave solution near the EK wave number in addition to the solution found near the EM plane wave propagation constant, but the contribution to the total infinite antenna current coming from the EK current wave is negligible in comparison with that due to the EM wave. A probably more important effect of the plasma compressibility on the antenna current is that the characteristic wave number near K_E which is real for the lossless, incompressible plasma, is complex for the compressible case. The fact that the current arising from the EK current wave is negligible for the infinite antenna does not rule out the possibility however, than the EK wave may be an important factor in connection with a finite cylindrical antenna. An antenna short compared with the EM wavelength but long in comparison with the EK wavelength may present a much greater impedance to the Fourier current components in the vicinity of the EM characteristic wave than to the EK characteristic wave, thus increasing the importance, of the EK contribution. The problem for the finite antenna really becomes one of finding $i_R(\beta)$ and $i_I(\beta)$, which for the free-space medium and a short antenna are well-approximated as a delta function at $\beta = K_{Eo}$. It should be mentioned that Wunsch (1967) obtained approximate solutions for the current on a short antenna in a compressible plasma, and found two components corresponding to the EM and EK characteristic waves.

It may also be remarked that above the plasma or hybrid frequency, the vacuum sheath has relatively little influence over the infinite antenna admittance. The vacuum sheath does have the effect however, of decreasing the magnitude of $i_R(\beta)$ near the characteristic wave solution at the EK wave number, and thus tends to decouple the antenna from the plasma compressibility. While this is relatively unimportant as far as the infinite antenna admittance is concerned, it may be a much more significant factor when the finite antenna is considered, especially if for the sheathless case, the EK waves assumes equal or major importance compared with the EM wave.

When the frequency is less than the upper hybrid or plasma frequency, the plasma compressibility and sheath are found to exert much greater control over the antenna admittance than for the situation discussed above, as also does the plasma anisotropy. Of particular interest is the fact that only when there is a sheath or the plasma is compressible is there a characteristic wave solution throughout the frequency range below the plasma or hybrid frequency. At the same time there is a strong similarity between the characteristic wave solutions for the incompressible, anisotropic, $5D_{\ell}$ vacuum sheath case and the compressible isotropic and anisotropic plasmas for the sheathless case.

The current on the infinite antenna is found to possess a wavelike nature with a propagation constant given by K_{zr} above f_p or f_t and below some lower cutoff frequency depending on the plasma model used. We define the cutoff frequency to mean here the frequency below which the current ratio is 0.5 or larger, so that the current has a rather well defined wave nature. In the case of the sheathless, incompressible anisotropic plasma, the cutoff frequency is f_h, while when there is a vacuum sheath, the cutoff frequency is more nearly $(f_h + f_t)/2$. For the compressible anisotropic plasma, the cutoff frequencies are also on the order of $(f_h + f_t)/2$. In the case of the compressible isotropic plasma, with or without a sheath, the cutoff frequency is about $0.9\ f_p$, so that the isotropic plasma antenna

current is wavelike for all frequencies except very near the plasma frequency. Because the characteristic wave numbers for this latter case are on the order of K_{Po} near f_p but rather rapidly approach K_{Eo} with decreasing frequency, it would appear that a finite antenna operated in this frequency range would exhibit a marked frequency dependence. When the anisotropic plasma is considered, the characteristic wave numbers are near K_{Eo} in the regions of wavelike antenna current, so that the electrical length of the antenna would not be so sensitive a function of frequency as for the isotropic plasma.

Since the current is of a generally evanescent nature in the frequency range above the cutoff frequency and below f_t or f_p, it might be expected that the infinite antenna and finite antenna admittances would be most alike in this range since the current reflections caused by the ends of the finite antenna become less important. This has indeed been found to be the case for the sheathless, incompressible isotropic and anisotropic cases, the results for which are given in I and II.

Besides affecting the infinite antenna admittance and current in some interesting aspects, the plasma compressibility has been found to produce a very significant alteration of the electric fields near the antenna, at the electron plasma frequency. The separate electric fields of the EM and EK modes are found to increase by two to three orders of magnitude at the plasma frequency, compared with their values on either side of it, but they are of nearly equal amplitude and opposite sign, to thereby maintain a relatively unchanged magnitude of the total electric field as a function of frequency. Because of the difference in the propagation velocities of the EM and EK waves, it appears that the total electric field near the antenna may consequently remain large, possibly even at first increasing in value, for a relatively long time after the antenna exciting voltage is removed, to provide a partial explanation for the relaxation resonance.

V. Summary and Conclusion

This investigation has been concerned with the properties of an infinite cylindrical antenna excited at a circumferential gap of non zero thickness and immersed in a lossy plasma medium. The antenna admittance was the topic of principal interest in I, II, and III (Miller 1967a; 1967b; 1967c) respectively where the plasma medium treated was isotropic and compressible, anisotropic and incompressible and anisotropic and compressible. In the present report the subject of primary concern has been the antenna current and near fields for the three plasma models used. An attempt has been made in the formulation of the problem, which proceeds from the linearized fluid equations for the electrons together with Maxwell's equations to account to some extent for the inhomogeneous ion sheath which forms about a body at floating potential in a warm plasma by including a concentric free-space layer, or vacuum sheath, between the antenna and the external uniform plasma. The antenna current and fields are obtained from a numerical evaluation of the appropriate Fourier integral, while the characteristic wave number solutions are found from the integrand of the current integral, with the numerical results being presented for plasma parameter values typical of the E region of the ionosphere.

The infinite antenna admittance has been found to be relatively unaffected by the plasma compressibility and vacuum sheath above the plasma frequency (f_p) for the isotropic plasma, or above the upper hybrid frequency (f_t), for the anisotropic plasma. Below these frequencies however, there are significant changes from the antenna admittance for the sheathless, isotropic, incompressibile plasma brought about by the plasma compressibility, vacuum sheath and plasma anisotropy, with the latter two fact ors appearing to be more influential in determining the antenna admittance than the plasma compressibility.

The more significant of the observed effects are: (1) The antenna admittance for the sheathless, isotropic, incompressible case is found to increase monotonically below the plasma frequency, whereas the presence of a vacuum sheath, plasma compressibility or plasma anisotropy results in one or more admittance maximum below f_t or f_p; (2) an admittance maximum which occurs at the electron cyclotron frequency (f_h) when there is no sheath is found to be shifted upward in frequency and reduced in magnitude by the presence of the vacuum sheath or the plasma compressibility; (3) an admittance minimum or kink is found at f_p for the anisotropic plasma; (4) the collision frequency dependence of the conductance in the isotropic plasma is lessened by the plasma compressibility; (5) the admittance is capacitive above f_p or f_t, is generally also capacitive below f_h for the anistropic plasma and may become capacitive sufficiently below f_p for the isotropic sheathed and/or compressible plasma, otherwise being inductive. It is interesting to mention that effects (2) and (3) have been observed in the measured admittance of an antenna operated in the ionosphere.

The antenna current is found to be wavelike with a propagation constant or wave number given approximately by the free-space plane wave EM propagation constant K_{Eo} multiplied by $\left[1-f_p^2/(f^2-f_h^2)\right]^{\frac{1}{2}}$, above f_p or f_t, for all the plasma models used. An additional current wave with a wave number near the EK plane wave propagation constant is found in the compressible plasma, but is is of negligible amplitude compared with the former current wave. Below f_h for the anisotropic plasma, or below approximately 0.9 f_p for the isotropic plasma whenever there is a vacuum sheath and/or the plasma is compressible, the current is again wavelike with a propagation constant which is larger than, but approaching, K_{Eo}. The effect of the sheath for all the plasma models used is to shift the current wave propagation constant closer to K_{Eo}, compared with the sheathless result.

While there may also exist characteristic wave number solutions in the intervening frequency range bounded by the frequencies given above, the total current is not then wavelike, but evanescent in the axial direction near the exciting gap. This may be expected to be an area then where the infinite and finite antenna admittances are most alike because the reflected currents from the ends of the finite antenna would be a minimum. This has indeed been found to be the case.

As a final area of investigation the antenna near-fields are found to be significantly altered for the isotropic plasma by the plasma compressibility. The individual EM and EK electric fields are sharply peaked, but of nearly equal magnitude and opposite phase, at the plasma frequency, so that the resultant electric field is much smaller than the separate components, being approximately the same as found in the incompressible plasma. Because of the large ratio of the EM to EK wave propagation velocity, the total electric field in the vicinity of an antenna in a compressible plasma may consequently exhibit at the plasma frequency an initial increase in value, or remain at a high level for a relatively long time after removing the antenna excitation. This field behavior provides a possible explanation for the relaxation resonance that has been observed in experimental ionospheric measurements.

In summary then, the infinite antenna analysis that has been undertaken in the present investigation has provided some numerical results that agree in a number of significant aspects with experimental measurements involving antennas immersed in the ionospheric plasma. In addition, the insight obtained from the infinite antenna current behavior may be helpful in further consideration of the admittance of a finite, plasma-immersed antenna.

Appendix A. Boundary Coupling of the EM and EK waves.

It has been pointed out above that as a consequence of using the rigid or hard boundary condition at the plasma interface, the EM and EK waves are coupled at the boundary. When however, the boundary is an absorbing one, and in the particular case where the boundary admittance is infinite (this is sometimes called the soft boundary), there is no boundary coupling. Consequently the antenna may excite the fields of both the EM and EK waves in the former case, and only the EM wave in the latter case. Actually, the boundary admittance need not be infinite, for the plasma parameter values of interest here, to negate the boundary coupling as a practical matter, but may have the finite admittance value derived by Balmain (1966) for what he called an absorptive boundary, and still be negligibly small.

This result is readily shown for the isotropic plasma, with or without a sheath. The velocity boundary condition may be written

$$v_\rho = Y_B n \Big|_{\rho=s} \tag{A1}$$

where v_ρ is the radially directed electron velocity, n is the time varying electron number density, Y_B is the surface admittance (after Cohen, 1962) and A1 is applied at the plasma-sheath interface, the quantities involved being evaluated in the plasma at $\rho=s$. Following the development of I, we can write (A1) as

$$\left[\frac{-i\lambda_P}{Y_B N^2} - \frac{m\omega\epsilon_o}{e^2} K_P{}^2 \frac{H_o^{(2)}(\lambda_P s)}{H_o^{(2)'}(\lambda_P s)} \right] H_o^{(2)'}(\lambda_P s)\, A_P + \frac{\lambda_E \beta}{K_E Y_B} H_o^{(2)'}(\lambda_E s) A_E = 0 \tag{A2}$$

where $H_o^{(2)}$ is a Hankel function of the second kind and order 0, the prime denotes differentiation with respect to argument, m and -e are the electron mass and charge, ϵ_o is the permittivity of free space and

$$K_E = K_{Eo}\sqrt{\epsilon_E}$$

$$K_P = K_{Po}\sqrt{\epsilon_E}$$

$$\lambda_E^2 = K_E^2 - \beta^2$$

$$\lambda_P^2 = K_P^2 - \beta^2$$

The electron collision frequency has been set equal to zero for simplification, and A_P and A_E are the Fourier coefficients for the transmitted EK and EM fields in the plasma outside the sheath that are produced by the antenna.

When Y_B is zero (the hard boundary) then A_E and A_P cannot be separately zero, thus demonstrating the coupling which the boundary brings about. If however, Y_B has a value of infinity in (A2), then it is obvious that A_P must be zero, so that in this case there is no EK field in the plasma, and the antenna excites only an EM field.

If we consider the intermediate value for Y_B derived by Balmain for the absorptive boundary, then we use

$$Y_B = \sqrt{2kT/\pi m}\ \frac{e^2}{\epsilon_o m\omega_p^2} \qquad \text{(A3)}$$

Upon rewriting (A1) in the form

$$A_P = \frac{\lambda_E \beta N^2}{-i\lambda_P K_E}\ \left[1+ m\omega\epsilon_o N^2 Y_B K_P^2 H_o^{(2)}(\lambda_P s)/i\lambda_P e^2 H_o^{(2)'}(\lambda_P s)\right]^{-1}\ \frac{H_o^{(2)'}(\lambda_E s)}{H_o^{(2)'}(\lambda_P s)} A_E$$

(A4)

we see that the magnitude of the term containing Y_B in the denominator of (A4) relative to unity will determine the influence of Y_B on the magnitude of A_P compared with A_E. Upon using a frequency of 2 MHz, a plasma frequency of 1.5 MHz and an electron temperature of 1,500°K, which correspond to the values used for the calculations, and noting that for small arguments,

$$\frac{H_o^{(2)}(x)}{H_o^{(2)'}(x)} \sim \frac{\pi X}{2i} \left[1 - \frac{i2}{\pi} \ln X\right]$$

the Y_B term in (A4) becomes approximately

$$\left| -i \frac{\omega s(1-N^2)}{\nu_r} \ln (\lambda_P s) \right| \approx 10 \qquad \text{(A5)}$$

In view of the value of (A5), we see that the Y_B term in the denominator of (A4) is generally dominant. This means that A_P is reduced in magnitude, in comparison with A_E, by an order of magnitude or more. Since A_E may be determined from the expressions given in I to be largely insensitive to Y_B (this is easily seen by observing that where $H_o^{(2)'}(\lambda_P s)$ appears in the expressions, it should be multiplied by the square bracket term in the denominator of (A4)), then we conclude that the EK field amplitudes are reduced by an order of magnitude or more for the absorptive boundary compared with the rigid boundary. Thus the effect of the boundary coupling to the EK mode is eliminated for practical purposes by the absorptive boundary since the compressibility has been found to be of negligible importance above f_p for the hard boundary, and the plasma compressibility is not "seen" by the antenna. Because the admittance is strongly influenced by the plasma compressibility below f_p however, Balmain's absorptive boundary admittance may not eliminate the compressibility effect.

A similar development may be followed to demonstrate that the soft boundary for the compressible, anisotropic plasma results in this case also in no boundary coupling of the EM and EK modes. An important difference in this case is however the fact that the anisotropic medium itself produces such coupling, so that even without the boundary contribution, an EK-type mode is excited by the antenna.

Finally, we may also note that when we use $Y_B = \infty$ for the soft boundary in (A1), it may be seen that for v_ρ to remain finite and thus satisfy the linearization, n must be zero at the boundary. If then the EM and EK waves are not coupled by the medium, there is no mechanism to produce a non zero n in the medium due to the non zero plasma temperature, so that the EK wave is not excited.

Appendix B. Conductance Dependence on Electron Temperature and Collision Frequency.

We want to discuss here the behavior of the antenna conductance, particularly below the plasma frequency, as a function of the electron temperature and collision frequency. In order to simplify the discussion, we will consider only the isotropic sheathless case, so that the antenna current at the exciting gap assumes the form

$$i_z(\beta) = \frac{-2\pi i \lambda_P U \; S(\beta) K_E c}{\eta N^2 \left[\frac{\lambda_P \lambda_E}{N^2} U \; \frac{H_o^{(2)}(\lambda_E c)}{H_o^{(2)'}(\lambda_E c)} + \beta^2 \; \frac{H_o^{(2)}(\lambda_P c)}{H_o^{(2)'}(\lambda_P c)} \right]} \qquad \text{(B1)}$$

where

$$\eta = \sqrt{\mu_o / \epsilon_o \epsilon_E}$$

$$\epsilon_E = 1 - \frac{N^2}{U}$$

$$\underline{\lambda}^2 = \underline{K}^2 - \beta^2$$

$$K_E^2 = \frac{\omega^2}{v_\ell^2} \epsilon_E$$

$$\epsilon_P = 1 - N^2 - i \frac{\nu}{\omega} = U - N^2 = 1 - N^2 - iZ$$

$$K_P^2 = \frac{\omega^2}{v_r^2} \epsilon_P$$

and the other symbols have been previously defined.

Since we are interested here in the case where $f < f_p$, then the Hankel function arguments are nearly pure imaginary (for small ν/ω). In addition, we will require the Hankel function arguments to be small, so that a suitable closed form expression may be employed for the Hankel functions. Since the λ's are nearly pure imaginary, we write

$$\frac{H_o^{(2)}(\lambda c)}{H_o^{(2)'}(\lambda c)} = - \frac{H_o^{(2)}(\lambda c)}{H_1^{(2)}(\lambda c)}$$

$$= i \frac{K_o(\tilde{\lambda} c)}{K_1(\tilde{\lambda} c)}$$

where

$$\lambda = -i\tilde{\lambda}$$

Now $K_o(z) \approx - \ln(\Gamma z/2)$

$$K_1(z) \approx \frac{1}{z}$$

where $\Gamma = 1.7811$

so $$\frac{H_o^{(2)}(\lambda_E c)}{H_o^{(2)}(\lambda_E c)} \approx -i \ln\left(\frac{\lambda_e c \Gamma}{2}\right) e^{i(\Delta_e' + \Delta_e)} \lambda_e c$$

$$\frac{H_o^{(2)}(\lambda_P c)}{H_o^{(2)'}(\lambda_P c)} \approx -i \ln\left(\frac{\lambda_p c \Gamma}{2}\right) e^{i(\Delta_p' + \Delta_p)} \lambda_p c$$

where $$\tilde{\lambda}_E = \sqrt{\beta^2 - K_E^2} \qquad \text{(B2)}$$

$$\approx \sqrt{\beta^2 - K_{Eo}^2 (1 - N^2 - iZ)}$$

$$\approx \sqrt{\beta^2 - K_{Eo}^2 (1-N^2)} \left\{1 + \left[\frac{iK_{Eo}^2 Z/2}{\beta^2 - K_{Eo}^2(1-N^2)}\right]\right\}$$

$$\approx \lambda_e e^{i\Delta_e}$$

and $$\tilde{\lambda}_P \approx \lambda_p e^{i\Delta_p} \qquad \text{(B3)}$$

with K_{Po} replacing K_{Eo} in (B2) to get (B3). Note that (B2) and (B3) require Δ_e and Δ_p to be small compared with unity. Also

$$\Delta_e' = \Delta_e \left[\ln(\lambda_e c \Gamma/2) \right]^{-1}$$

$$\Delta_p' = \Delta_p \left[\ln(\lambda_p c \Gamma/2) \right]^{-1}$$

Then $i_z(\beta)$ may be written as

$$i_z(\beta) \approx \frac{-2\pi i\, S(\beta)\, \omega \epsilon_o \left[1 - N^2 - iZ(2-N^2) \right]}{N^2 \left[-\lambda_e^2 \ln(\lambda_e c \Gamma/2) \exp(2i\Delta_e + i\Delta_e' - iZ)/N^2 \right.}$$

$$\left. + \beta^2 \ln(\lambda_p c \Gamma/2) \exp(i\Delta_p') \right] \qquad \text{(B4)}$$

Now for small electron temperatures, such that

$$K_{Eo} \lesssim 10^{-3} K_{Po}$$

then $$\Delta_p \approx \frac{Z}{2(N^2 1)} >> \Delta_e \approx \frac{K_{Eo}^2 Z}{2\beta^2}$$

for $$K_{Eo} << \beta \lesssim K_{Po}$$

which is in the area of the current peak at f=1.4 MHz (see Fig. 7). Thus the denominator of (B4) becomes

$$\left[\quad \right] \approx \beta^2 \left[\ln(\lambda_p c \Gamma/2) - \ln(\lambda_e c \Gamma/2)/N^2 \right.$$

$$\left. + K_{Eo}^2 (1-N^2) \ln(\lambda_e c \Gamma/2)/N^2 \right.$$

$$\left. + i\beta^2 \Delta_p' \right]$$

$$= d_r + i d_i \qquad \text{(B5)}$$

Then the real current component is written

$$i_R(\beta) = \mathrm{Re}\ \frac{C\left\{-Z(2-N^2)-i(1-N^2)\right\}}{d_r + id_i} \qquad (B6)$$

$$= \mathrm{Re}\ \frac{n_r + i\,n_i}{d_r + i\,d_i}$$

$$= \frac{n_r d_r + n_i d_i}{d_r^2 + d_i^2}$$

We note that d_i and n_r are proportional to ν, so that when

$$\nu = 0,$$

$$d_i = n_r = 0$$

and the current is pure imaginary, i.e., the conductance is then zero. It may be noted that when d_r is zero (this is the characteristic wave solution which is discussed more fully in Appendix C), then

$$i_R(\beta_o) = \frac{n_i}{d_i}$$

and that i_R may apparently become infinite when $\nu = 0$, in contradiction to the previous observation. This is an example of a double limit process where two apparently different answers can be obtained depending on the order in which the limits are taken. Note that when Z=0, then $i_I(\beta)$ becomes infinite when $d_r=0$.

The general behavior of the $i_R(\beta)$ curve shown in Fig. 7 is in agreement with (B6). The portion of the curve away from the $d_r = 0$ area is proportional to ν, while the peak value appears to be in proportion to ν.

If we now consider the limit of vanishing electron temperature, then in order to ensure the Hankel function approximation validity, we will require that

$$K_P c << 1$$

$$\lim v_r \to 0$$

and we note $\lim_{v_r \to 0} K_P \to \infty$

We are thus required to have the cylinder radius vanish as fast as the electron velocity. In this case then, the denominator given by (B5) becomes

$$\left[\quad\right] \sim \frac{1}{N^2}\left[-\beta^2 - K_{E_o}^2(1-N^2)\right] \ln(\lambda_e c\Gamma/2) + i\,\beta^2\Delta_p$$

and we observe that now $d_i/d_r \to 0$ as $c \to 0$.

Thus $\lim_{\substack{v_r \to 0 \\ c \to 0 \\ f < f_p}} i_R(\beta) \approx \frac{n_r}{d_r} \propto Z$

which is the cold plasma result.

If on the other hand, we keep c constant as $v_r \to 0$, then we may use the large argument forms for the Hankel functions since we know that the peak in β is near K_P, to get

$$\lim_{v_r \to 0} \frac{H_o^{(2)}(\lambda_- c)}{H_o^{(2)'}(\lambda_- c)} = i$$

so that the current may be approximated by,

$$i_z(\beta) \approx \frac{-i2\pi c\epsilon_o S(\beta)\omega\left[1-N^2-iZ(2-N^2)\right]}{N^2\left[-\beta^2/\lambda_p e^{i\Delta_p} + \lambda_e e^{i\Delta_e}/N^2\right]} \qquad \beta \sim K_P \qquad \text{(B7)}$$

As before, we note that $\Delta_p >> \Delta_e$ so that the denominator is approximately

$$\left[\quad\right] \approx \frac{\lambda_e}{N^2} - \frac{\beta^2 e^{-i\Delta_p}}{\lambda_p}$$

We note that the real part of the denominator becomes zero when

$$\frac{\lambda_e}{N^2} = \frac{\beta_o^2}{\lambda_p}$$

so that

$$\beta_o^2 = \frac{K_{Po}^2}{(1+N^2)} \tag{B8}$$

It may be seen that $i_R(\beta) \propto Z$ when the real part of the denominator of (B7) is much larger than the imaginary part, while $i_R(\beta) \propto Z^{-1}$ when the converse is true. This is the behavior exhibited by the graphical $i_R(\beta)$ results. In order to estimate the peak contribution from the area of the β_o value given by (B8) to the total real antenna current, we first write

$$\beta = \frac{K_{Po}}{\sqrt{1+N^2}} (1 \pm \Delta) \quad ; \Delta << 1 \tag{B9}$$

and solve for the value of Δ at which the real and imaginary denominator components are equal. We find that

$$\Delta (N^4-1) = \Delta_p N^4 (1-2\Delta + \Delta/N^4)$$

and using the value of Δ_p from (B3), there is obtained

$$\Delta \approx \frac{Z}{2(N^2-1)} \tag{B10}$$

Thus, when Δ exceeds the value given by (B10), the denominator of (B7) is donimant and $i_R(\beta) \propto Z$, but when Δ is less than this value then $i_R(\beta) \propto Z^{-1}$.

We then approximate the integration of $i_R(\beta)$ through the peak by

$$I_R(z) \propto Z^{-1} \int_{\beta_o(1-\Delta)}^{\beta_o(1+\Delta)} S(\beta) \cos(\beta z)\, d\beta \tag{B11}$$

Since $\beta_o \sim K_{P_o}$ and we are interested in the limit $v_r \rightarrow 0$, then $\beta_o \delta >> 1$ for small enough v_r. In addition the change in β over the range of integration of (B11) is $2\ \beta_o \Delta$, so that the argument of the $\sin(\beta \delta/2)$ term in $S(\beta)$ changes by $\beta_o \Delta \delta$. If $\beta_o \Delta \delta \leq \pi$ and $z = \delta/2$ so the $\cos(\beta z)$ term is also relatively constant, then approximately,

$$I_R(\delta/2) \propto Z^{-1} \int_{\beta_o(1-\Delta)}^{\beta_o(1+\Delta)} d\beta/\beta \qquad \text{(B12)}$$

$$= Z^{-1} \ln\left(\frac{1+\Delta}{1-\Delta}\right)$$

$$\approx Z^{-1} 2\Delta = \frac{1}{(N^2-1)}$$

If on the other hand, $\beta_o \Delta \delta >> \pi$, then

$$I_R(\delta/2) \propto Z^{-1} \int_{+\beta_o(1-\Delta)}^{\beta_o(1+\Delta)} \sin(\beta\delta/2) \cos(\beta\delta/2)\, d\beta / \beta$$

which because of the oscillation of the sine and cosine terms is less than (B12), and as $v_r \rightarrow 0$ then also $I_R \rightarrow 0$.

Thus, for a non zero electron velocity, and small collision frequency, the current from the peak at β_o is not very sensitive to the collision frequency. When however, the velocity becomes vanishingly small, the peak current also becomes vanishingly small, and contributes negligibly to the total current, or the antenna conductance.

Appendix C. Approximate Characteristic Wave Number Solutions.

In this appendix, we discuss the characteristic wave solutions for the various isotropic plasma models considered above. In particular an approximate expression is obtained for the characteristic wave number from the integrand of the Fourier current integral, for the sheathless case, while the modification of the sheathless result brought about by the vacuum sheath is also examined. We will deal with, in order, the sheathless incompressible and compressible plasma cases, followed by the vacuum sheath incompressible and compressible plasmas.

(1) The sheathless, incompressible plasma.

The Fourier current may be written as

$$i_z(\beta) = (2\pi i c K_E S(\beta)/\eta \lambda_E) H_o^{(2)'}(\lambda_E c)/H_o^{(2)}(\lambda_E c) \qquad (C1)$$

where the various quantities have been previously defined. It may be seen that $i_z(\beta)$ becomes infinite when

$$\lambda_E = 0$$

Thus,

$$\beta_o = K_E = \frac{\omega}{v_\ell}\sqrt{\epsilon_E} \qquad (C2a)$$

which becomes for $Z << |1-N^2|$

$$\beta_o \approx \frac{\omega}{v_\ell}\sqrt{1-N^2}\left(1 - \frac{iZ}{2(1-N^2)}\right) \qquad (C2b)$$

It is apparent that β_o is nearly pure real above f_p and nearly pure imaginary below it, becoming pure real and pure imaginary respectively when $\nu = 0$. The behavior indicated by (C2b) is exhibited by the results of Fig. 11.

(2) The sheathless, compressible plasma.

In this case, the Fourier current may be expressed as

$$i_z(\beta) = \frac{2\pi i S(\beta) K_E}{\lambda_E \eta} \frac{H_o^{(2)'}(\lambda_E c)}{H_o^{(2)}(\lambda_E c)} \frac{1}{D(\beta)} \qquad (C3)$$

$$D(\beta) = 1 + \frac{\beta^2 N^2}{U\lambda_P\lambda_E} \frac{H_o^{(2)}(\lambda_P c)}{H_o^{(2)'}(\lambda_P c)} \frac{H_o^{(2)'}(\lambda_E c)}{H_o^{(2)}(\lambda_E c)} \tag{C4}$$

If we consider the collisionless case, it may be concluded that $D(\beta) \neq 0$ unless the Hankel function arguments are pure imaginary. This means that either $f < f_p$ or $f > f_p$ and $\beta > K_P$. Assuming small (compared with unity) imaginary arguments so that

$$\frac{H_o^{(2)'}(-ix)}{H_o^{(2)}(-ix)} \sim \frac{i}{x\ln(x\Gamma/2)}$$

then we have

$$D(\beta) = 0 = \left[-\lambda_e^2 \ln(\lambda_e c\Gamma/2)/N^2 + \beta^2 \ln(\lambda_p c\Gamma/2) \right] \tag{C5}$$

where λ_e and λ_p are given by (B2) and (B3). Thus, β_o is a solution to $D(\beta) = 0$ or

$$\beta_o^2 = \frac{K_{Eo}^2(1-N^2)}{1 - N^2 \frac{\ln(\lambda_p c\Gamma/2)}{\ln(\lambda_e c\Gamma/2)}} \tag{C6}$$

and we have a transcendental relationship for β_o. But since for $f > f_p$, $\beta_o^2 \sim K_P^2 >> K_{Eo}^2$, then the denominator of (C5) must be nearly zero, so

$$N^2 \frac{\ln(\lambda_p c\Gamma/2)}{\ln(\lambda_e c\Gamma/2)} \cong 1 \tag{C7}$$

or

$$(\lambda_p c\Gamma/2)^{N^2} = (\lambda_e c\Gamma/2)$$

This can be written as

$$\left[\beta_o^2 - K_{Po}^2(1-N^2) \right] N^2 \left(\frac{c\Gamma}{2} \right)^{2N^2} = \left[\beta_o^2 - K_{Eo}^2(1-N^2) \right] \left(\frac{c\Gamma}{2} \right)^2$$

$$\approx \left(\frac{\beta_o c\Gamma}{2} \right)^2 \tag{C8}$$

Rearranging, we obtain

$$\beta_o^2\left[(\beta_{oc}\Gamma/2)^{\frac{2}{N^2}-2}-1\right] = -K_{Po}^2(1-N^2)$$

But if $N^2 < 1$ (i.e., $f > f_p$), then $2/N^2 > 2$ and since $K_{Po}c \ll 1$ is assumed, we get

$$\beta_o^2 = K_{Po}^2(1-N^2) \qquad \text{(C9)}$$

which checks the results of Fig. 11 quite well.

The solution obtained by Seshadri (1964), is

$$\beta_o^2 = K_{Po}^2(1+N^2)^{-1}$$

and when $N^2 \ll 1$, this is approximately

$$\beta_o^2 \cong K_{Po}^2(1-N^2)$$

in agreement with (C9).

If rather than $N^2 < 1$, we have $1 \lesssim N^2$, then approximately

$$\beta_o^2 \approx \left[K_{Po}\sqrt{N^2-1}\,\frac{c\Gamma}{2}\right]^{2N^2}\left(\frac{c\Gamma}{2}\right)^{-2} \qquad \text{(C10)}$$

As an example, when $N^2 = 2$, β_o from (C10) is 5.1 m^{-1} while from Fig. 11, K_{zr} is 4.7 m^{-1}. For $N^2 = 3$, (C10) produces 1.7 m^{-1} while K_{zr} from Fig. 11 is 1.2 m^{-1}.

As N^2 gets larger, (C10) becomes less accurate, since K_{Eo}^2 has been neglected in (C8) compared with β_o, which approaches K_{Eo} for large enough N^2. Thus we see from (C6), that as N^2 becomes large enough, then since

$$\lambda_p^2 \approx K_{Po}^2 N^2$$

$$\lambda_e^2 \approx K_{Eo}^2 N^2$$

the log ratio in the denominator of (C6) approaches a constant less than unity which is independent of β, and β_o^2 is close to, but larger than K_{Eo}^2, given by

$$\beta_o^2 = K_{Eo}^2 \ln(\lambda_e c\,\Gamma/2) \,/\ln(\lambda_p c\,\Gamma/2)$$

We have so far examined (C4) for the root near K_{Po} when $f > f_p$. It may be seen however, that there is another root which is not however, pure real, located near K_{Eo}. If we consider the case where $v_r \to 0$ so that the large argument approximations may be used for the Hankel functions whose argument involve λ_P, then $D(\beta) = 0$ becomes, again assuming $\lambda_E c$ small and imaginary,

$$-\lambda_e^2 c \ln(\lambda_e c\,\Gamma/2)\,/N^2 - \beta_o^2/\lambda_P = 0 \qquad \text{(C11)}$$

We obtain β_o^2 as

$$\beta_o^2 \approx \frac{K_{Eo}^2\,(1-N^2)}{1+N^2/\left[K_{Po}(1-N^2)c\,\ln(\lambda_e c\,\Gamma/2)\right]} \qquad \text{(C12)}$$

Since $K_{Po} c >>$ is assumed in obtaining (C12), we see that

$$\beta_o^2 \approx K_{Eo}^2(1-N^2) \qquad \text{(C13)}$$

Thus, in the limit of vanishing electron temperature, a characteristic wave solution is found which agrees with the incompressible result given by (C2b).

If we consider the case where the small argument forms may be used for the Hankel functions, e.g. the cylinder radius may be made arbitrarily small, then (C4) becomes again for λ_E imaginary,

$$D(\beta) = 0 = c\left\{-\lambda_e^2 \ln(\lambda_e c\,\Gamma/2)/N^2 + \frac{i\pi}{2}\beta_o^2\left[1 - \frac{i2}{\pi}\ln(\lambda_P c\,\Gamma/2)\right]\right\} \qquad \text{(C14)}$$

We observe that (C14) may not be satisfied in general for a pure real value of β_o. If however, the limit $c \to 0$ is examined, the solution approaches a pure real value. Solving for β_o^2 from (C14), there is obtained

$$\beta_o^2 = \frac{K_{Eo}^2\,(1-N^2)}{1-N^2\left[\frac{i\pi}{2} + \ln(\lambda_P c\,\Gamma/2)\right]\,/\,\ln(\lambda_e c\,\Gamma/2)} \qquad \text{(C15)}$$

which is again a transcendental expression, for β_o^2. We note that the K_{zr} values presented in the report are the β values for which the real part of (C14) are zero, or

$$K_{zr}^2 = \frac{K_{Eo}^2 (1-N^2)}{1-N^2 \ln(\lambda_P c\Gamma/2)/\ln(\lambda_e c\Gamma/2)} \qquad \text{(C16)}$$

which has the same form as (C6). If

$$N^2\pi/2 << \left| \ln(\lambda_e c\Gamma/2) - N^2 \ln(\lambda_P c\Gamma/2) \right|$$

then it appears that K_{zr}^2 is a good approximation to real (β_o^2).

It is thus seen that the plasma compressibility, in addition to leading to a characteristic wave number solution near K_{Po}, changes the real incompressible plasma characteristic wave soltuion at K_E to a complex number whose real part is approximately equal to K_E. A detailed examination of the integrand of the Fourier integral for the current, as is presented in Section III a. shows however, that the infinite antenna current for the compressible plasma is dominated by the contribution coming from the peak near K_E, even though the characteristic wave number for this current wave is complex rather than real, as is the case for the current wave whose wave number is near K_{Po}. When the electron temperature or the cylinder radius approaches zero, then the wave number near K_E becomes real.

(3) The vacuum sheath, incompressible plasma.

The Fourier current then has the form

$$i_z(\beta) = -\frac{iS(\beta)}{\lambda_E \eta} 2\pi c K_E \frac{H_o^{(2)'}(\lambda_E s)}{H_o^{(2)}(\lambda_E s)} \frac{W(c,'s)}{W(c,s')} \frac{1}{D(\beta)} \left\{ 1 - \frac{\lambda_E K_{Eo} \eta}{\lambda_{Eo} K_E \eta_o} \frac{H_o^{(2)}(\lambda_E s)}{H_o^{(2)'}(\lambda_E s)} \frac{W(c', s')}{W(c', s)} \right\} \qquad \text{(C17)}$$

where

$$D(\beta) = 1 - \frac{\lambda_{Eo}\eta_o K_E}{\lambda_E \eta K_{Eo}} \frac{H_o^{(2)'}(\lambda_E s)}{H_o^{(2)}(\lambda_E s)} \frac{W(c, s)}{W(c, s')} \qquad \text{(C18)}$$

and the W functions have the form

$$W(c^*, s^+) = H_o^{(1)*}(\lambda_{Eo}c)\ H_o^{(2)+}(\lambda_{Eo}s) - H_o^{(2)*}(\lambda_{Eo}c)\ H_o^{(1)+}(\lambda_{Eo}s)$$

where the $^+$ and * are primes or blanks in (C17) and (C18) to denote differentiation with respect to argument or lack of it, as the case may be. Also

$$\lambda_{Eo}^2 = K_{Eo}^2 - \beta^2$$

and s denotes the sheath radius. It may be verified that when s=c, i.e. the sheathless case, then (C17) and (C18) reduce to (C1), since then $W(c, s) = W(c', s') = 0$ and $W(c, s') = -W(c', s)$.

Before we can examine the behavior of $D(\beta)$, it is necessary to determine the properties of the W-functions for real or imaginary arguments. Because

$$H_n^{(1, 2)}(X) = J_n(X) \pm i\, N_n(X)$$

where J_n and N_n are the Bessel and Neumann functions, we can show that

$$W(c^*, s^+) = 2i \left[J_o^+(\lambda_{Eo}s)\, N_o^*(\lambda_{Eo}c) - J_o^*(\lambda_{Eo}c)\, N_o^+(\lambda_{Eo}s) \right] \qquad \text{(C19)}$$

Thus for real λ_{Eo}, it is obvious that all the W-functions are imaginary.

When however, the arguments are imaginary, then since the negative root must be used, we have

$$H_n^{(2)}(-iX) = \frac{2}{\pi}\, i^{n+1}\, K_n(X)$$

$$H_n^{(1)}(-iX) = 2\,(-i)^n\, I_n(X) + \frac{2}{\pi}\, i^{n-1} K_n(X)$$

where I_n and K_n are the modified Bessel functions of the first and second kind respectively. Thus we may deduce that for imaginary arguments, $W(c, s)$, and $W(c', s')$ are imaginary, while $W(c', s)$ and $W(c, s')$ are real. The properties of the W-functions may be summarized as:

Real Arguments		Imaginary Arguments	
$W(c, s) < 0$	Imaginary	$W(c, s) < 0$	Imaginary
$W(c', s') < 0$		$W(c', s') < 0$	
$W(c', s) > 0$		$W(c', s) < 0$	Real
$W(c, s') < 0$		$W(c, s') > 0$	

An examination of (C18) for $f > f_p$ shows that $\beta > K_E$ is required for the Hankel function ratio not to be complex, the ratio being then negative imaginary. If $\beta < K_{Eo}$ then, the W-function ratio is positive real, while λ_E is negative imaginary, so that the second term is $D(\beta)$ is positive real. Thus $D(\beta)$ can become zero, and a characteristic wave solution is expected only for $K_E < \beta < K_{Eo}$ when $f > f_p$, the two terms in (C18) being otherwise additive. Since, for small arguments,

$$W(c, s) \cong \frac{4i}{\pi} \ln(c/s)$$

and

$$W(c, s') \approx -\frac{4i}{\pi \lambda_{Eo} s}$$

$$\frac{H_o^{(2)'}(\lambda_E s)}{H_o^{(2)}(\lambda_E s)} \approx \frac{i}{s\lambda_e \ln(\lambda_e s \Gamma/2)}$$

so that

$$D(\beta) = 0 = 1 - \frac{\epsilon_E \lambda_{Eo}}{\lambda_E} \frac{i}{s\lambda_e \ln(\lambda_e s \Gamma/2)} \frac{4i}{\pi} \ln(c/s) - \frac{\pi \lambda_{Eo} s}{4i} \tag{C20}$$

and

$$\lambda_e^2 \ln(\lambda_e s \Gamma/2) = \epsilon \lambda_{Eo}^2 \ln(c/s) \tag{C21}$$

Thus $$\beta_o^2 = K_{Eo}^2 \epsilon_E \left[\frac{\ln(\lambda_e s\Gamma/2) + \ln(c/s)}{\ln(\lambda_e s\Gamma/2) + \epsilon_E \ln(c/s)} \right] \qquad (C22)$$

$$= \frac{K_{Eo}^2 \epsilon_E}{1 - N^2 \ln(c/s)/\ln(\lambda_e c\Gamma/2)}$$

It may be seen that when c=s, then (C22) reduces to sheathless result given by (C2b), and for zero collision frequency, β_o is pure real. In addition, since the log arguments are less than 1, then the log terms in (C22) are negative, and because $\epsilon_E < 1$, then the bracket in (C22) is positive and greater than unity, so that β_o is indeed larger than K_E. A further examination of (C18) for the case $\beta > K_{Eo}$ reveals that the second term adds to the first, so $D(\beta)$ has no zero then and there is no characteristic wave solution in this range. Finally, the results of Figure 11 may be seen to be in agreement with (C22).

If we now consider the case where $f < f_p$, then again utilizing our knowledge of the behavior of the W-functions and other factors in (C18), it may be concluded that $\beta > K_{Eo}$ is required for a solution to $D(\beta) = 0$. The small argument approximations for the Hankel and W-functions leads to the same expression for β_o^2 for $f < f_p$ as was found for $f > f_p$, as given by (C22). Since the values obtained for K_{zr} as shown on Fig. 11 become much larger than K_{Eo} near f_p, it appears that the denominator of (C22) must be nearly zero for $\beta_o >> K_{Eo}$, and thus

$$\beta_o^2 \approx \left(\frac{2}{s\Gamma}\right)^2 \left(\frac{c}{s}\right)^{2|\epsilon_E|} + K_E^2 \qquad (C23)$$

so that when f is near f_p

$$\beta_o^2 \approx \frac{2}{s\Gamma} \qquad (C24)$$

This turns out to be a fairly good approximation to K_{zr} since $K_{zr} \sim 10^1$ near f_p while (C25) yields $\beta_o \sim 10^1$ also (s here is 0.089 m). As N^2 gets larger, the (c/s) term in (C23) rapidly reduces β_o^2 in value, which is in agreement with the graph on Fig. 11. When N^2 becomes sufficiently large, then (C22) becomes approximately

$$\beta_o^2 \approx K_{Eo}^2 \left[1 + \ln(\lambda_e s \Gamma/2) \; / \; \ln(c/s) \right]$$

and β_o^2 is observed to approach K_{Eo}.

It is also of interest to see how β_o behaves when the arguments $\lambda_E s$, etc. are large so that we may use, as a first approximation, the large argument Hankel function expressions. In this case,

$$\frac{H_o^{(2)'}(\lambda_E s)}{H_o^{(2)}(\lambda_E s)} \approx -i$$

$$W(c, s) \approx -\frac{4i}{\pi} \frac{\sinh\left[\lambda_{eo}(s-c)\right]}{\lambda_{eo}\sqrt{cs}}$$

$$W(c, s') \approx \frac{4}{\pi} \frac{\cosh\left[\lambda_{eo}(s-c)\right]}{\lambda_{eo}\sqrt{cs}}$$

where $\lambda_{eo}^2 = \beta^2 - K_{Eo}^2$

Thus

$$D(\beta) = 0 = 1 - \frac{\lambda_{eo}}{\lambda_e} \epsilon_E (-i) \left\{ \frac{-i \sinh\left[\lambda_{eo}(s-c)\right]}{\cosh\left[\lambda_{eo}(s-c)\right]} \right\} \qquad \text{(C25)}$$

so $$\lambda_e = -\lambda_{eo} \epsilon_E \tanh\left[\lambda_{eo}(s-c)\right]$$

and $$\beta_o^2 = K_{Eo}^2\ \epsilon_E \left\{ \frac{1 - \epsilon_E \tanh^2 \left[\lambda_{eo}(s-c)\right]}{1 - \epsilon_E^2 \tanh^2 \left[\lambda_{eo}(s-c)\right]} \right\}$$

$$\approx K_{Eo}^2\ \epsilon_E \left[\frac{1 - \epsilon_E}{1 - \epsilon_E^2} \right]$$

$$= K_{Eo}^2\ \epsilon_E / (1 + \epsilon_E) = K_{Eo}^2\ (1 - N^2) / (2 - N^2) \qquad \text{(C26)}$$

The approximate expression for β_o^2 is seen to provide a real solution only when $N^2 > 2$ and indicates that a maximum value may be expected at $N^2 = 2$. The curve on Fig. 11 for this case has a maximum for N^2 between 1.55 and 1.15. Evidently, the approximations used in deriving (C26) have resulted in an expression for β_o^2 which is only qualitatively correct. It appears from (C25), that the thicker the sheath, the more nearly correct will be (C26).

(4) The vacuum sheath, compressible plasma.

In this case we obtain

$$i_z(\beta) = -\frac{iS(\beta)}{\lambda_E \eta} \frac{H_o^{(2)'}(\lambda_E s)}{H_o^{(2)}(\lambda_E s)} \frac{W(c', s)}{W(c, s')} \frac{2\pi c K_E}{D(\beta)} \left\{ 1 - \frac{W(c', s')}{W(c', s)} \left[\frac{\eta K_{Eo} \beta^2 N^2}{\lambda_{Eo} \eta_o K_E \lambda_P U} \frac{H_o^{(2)}(\lambda_P s)}{H_o^{(2)'}(\lambda_P s)} + \frac{\eta K_{Eo} \lambda_E}{\eta_o K_E \lambda_{Eo}} \frac{H_o^{(2)}(\lambda_E s)}{H_o^{(2)'}(\lambda_E s)} \right] \right\} \qquad \text{(C27)}$$

with $$D(\beta) = 1 + \frac{\beta^2 N^2}{\lambda_P \lambda_E U} \frac{H_o^{(2)}(\lambda_P s)}{H_o^{(2)'}(\lambda_P s)} \frac{H_o^{(2)'}(\lambda_E s)}{H_o^{(2)}(\lambda_E s)} \qquad \text{(C28)}$$

$$- \frac{\eta_o K_E \lambda_{Eo}}{\eta K_{Eo} \lambda_E} \frac{H_o^{(2)'}(\lambda_E s)}{H_o^{(2)}(\lambda_E s)} \frac{W(c, s)}{W(c, s')}$$

It may again be verified that (C27) reduces to each of the special cases previously considered when $v_r \to 0$ and/or $s \to c$. Since the plasma compressibility has resulted in adding a new term to each of the numerator and denominator of $i_z(\beta)$ compared with the incompressible case of (C17), it should suffice to examine these new terms.

The observations previously made for the sheathless, compressible plasma also apply here in that even with zero electron collision frequency, there is no possibility for a zero in $D(\beta)$ when $f > f_p$ unless $\beta > K_P$. Again using the small argument forms for the Hankel functions we find from (C26) that, for $\beta > K_P$,

$$D(\beta) = 0 = 1 - \frac{\lambda_{eo}}{\lambda_e} \epsilon_E \left[\frac{i}{s\lambda_e \ln(\lambda_e s \Gamma/2)} \right] \left[i \ln(c/s) \lambda_{eo} s \right]$$

$$- \frac{\beta_o^2 N^2}{\lambda_p \lambda_e} \left[\frac{\lambda_p s \ln(\lambda_p s \Gamma/2)}{\lambda_e s \ln(\lambda_e s \Gamma/2)} \right]$$

or
$$1 = -\epsilon_E \frac{\lambda_{eo}^2}{\lambda_e^2} \frac{\ln(c/s)}{\ln(\lambda_e s \Gamma/2)} + \frac{\beta_o^2 N^2}{\lambda_e^2} \left[\frac{\ln(\lambda_p s \Gamma/2)}{\ln(\lambda_e s \Gamma/2)} \right] \quad \text{(C29)}$$

and
$$\beta_o^2 = \frac{K_{Eo}^2 (1-N^2) \left[\ln(c/s) / \ln(\lambda_e s \Gamma/2) + 1 \right]}{1 - N^2 \ln(\lambda_p s \Gamma/2) / \ln(\lambda_e s \Gamma/2) + \epsilon_E \ln(c/s) / \ln(\lambda_e s \Gamma/2)}$$

$$= \frac{K_{Eo}^2 (1-N^2)}{1 - N^2 \ln(\lambda_p c \Gamma/2) / \ln(\lambda_e c \Gamma/2)} \quad \text{(C30)}$$

This expression is also valid when $f < f_p$ and $\beta > K_{Eo}$; if $\beta < K_{Eo}$, then $D(\beta)$ has no zero. The special cases considered previously may be obtained from (C30) by letting $v_r \to 0$ and/or $s \to c$.

It is interesting to note that to a first approximation, the sheath does not shift the value of β_o^2, as a comparison of (C30) and (C6) shows. Again noting that (C30) is derived for $\beta > K_P$, then the denominator of (C30) must be nearly zero, and consequently

$$\ln(\lambda_e s \Gamma/2) + \epsilon_E \ln(c/s) - N^2 \ln(\lambda_p s \Gamma/2) = 0 \qquad \text{(C31)}$$

or $$\frac{(\lambda_e s \Gamma/2)\,(c/s)^{\epsilon_E}}{(\lambda_p s \Gamma/2)^{N^2}} = 1$$

and since $\beta_o \sim K_P >> K_E$, then

$$\beta_o^2 \left[1 - \left(\frac{\beta_o s \Gamma}{2} \right)^{\frac{2}{N^2}-2} \left(\frac{c}{s} \right)^{\frac{2\epsilon_E}{N^2}} \right] = K_{Po}^2 (1-N^2) \qquad \text{(C32)}$$

which is the same as (C8) except for the (c/s) term. If $N^2 < 1$, then we find from (C32) approximately the same expression for β_o^2 as given by (C9). If however $1 < N^2$, then (C32) yields

$$\beta_o^2 \approx \left[K_{Po} \sqrt{N^2-1} \left(\frac{s\Gamma}{2} \right)^{2N^2} \left(\frac{s}{c} \right)^{2\epsilon_E} \left(\frac{2}{s\Gamma} \right)^2 \right]$$

$$= \left[K_{Po} \sqrt{N^2-1} \left(\frac{c\Gamma}{2} \right)^{2N^2} \left(\frac{2}{c\Gamma} \right) \right] \qquad \text{(C33)}$$

We thus find that with the approximations used here, the sheath does not affect the value of β_o^2, when the plasma is compressible, in contradiction to our numerical results. However, in this derivation the small argument forms have been used for the Hankel functions, and since $\lambda_P s \sim 1$ or larger near f_p, these approximations are evidently not too good as far as the numerical calculations are concerned.

If we consider $f > f_p$ and $K_E < \beta < K_{Eo}$ as before, then $D(\beta)$ becomes

$$D(\beta) = 0 = 1 + \epsilon_E \frac{\lambda_{Eo}}{i\lambda_e}\left[\frac{i}{s\lambda_e \ln(\lambda_e s\Gamma/2)}\right]\left[-\ln(c/s)\lambda_{Eo}s\right]$$

$$+ \frac{\beta_o{}^2 N^2}{\lambda_P(-i\lambda_e)}\left[\frac{i}{s\lambda_e \ln(\lambda_e s\Gamma/2)}\right]\left[\frac{1 - \frac{2}{\pi} i \ln(\lambda_P s\Gamma/2)}{-\frac{2i}{\pi\lambda_P s}}\right]$$

or
$$\lambda_e{}^2 \ln(\lambda_e s\Gamma/2) - \epsilon_E \lambda_{Eo}{}^2 \ln(c/s) - \frac{i\pi}{2}\beta_o{}^2 N^2\left[1 - \frac{2}{\pi} i \ln(\lambda_P s\Gamma/2)\right] = 0 \qquad \text{(C34)}$$

Again noting that $K_{zr} = \mathrm{Re}(\beta_o)$ is obtained from the β_o where the real part of (C32) is zero, we get

$$K_{zr}{}^2 \simeq \frac{K_{Eo}{}^2(1-N^2)\left[\ln(\lambda_e s\Gamma/2) + \ln(c/s)\right]}{\ln(\lambda_e s\Gamma/2) - N^2 \ln(\lambda_P s\Gamma/2) + \epsilon_E \ln(c/s)} \qquad \text{(C35)}$$

the same in form as (C30) except here we have $K_E < \beta < K_{Eo}$ rather than $\beta > K_P$ as for (C30).

(5) Anistropic Plasma.

This case has been examined by Lee and Lo (1967) for the incompressible, sheathless plasma, as mentioned in the text. When however, we consider the vacuum sheath, anisotropic incompressible plasma, or the sheathless, anisotropic compressible plasma, the current expressions become extremely complicated. Consequently, the derivation of a relatively simple form for β_o is quite difficult and is not attempted here. The results shown on Fig. 10 and 12 show however, the general trend of the characteristic wave solutions when the plasma is anisotropic and/or compressible and for the incompressible case, show the effect of the vacuum sheath. The results obtained here pertaining to the characteristic wave numbers are briefly summerized below.

(6) Summary.

The approximate expressions derived here for the characteristic wave solutions, together with the numerical results presented for K_{zr} in section III 2 show the following general behavior.

(a) The Sheathless Case.

When the plasma is incompressible, and isotropic, the characteristic wave number is equal to $K_{Eo}\sqrt{\epsilon_E}$ and thus is real for only the case $f > f_p$. For the anisotropic incompressible plasma, the wave number is approximately $K_{Eo}\sqrt{1-N^2/(1-H^2)}$ and is real for $f > f_t$ and $f < f_h$. When the plasma is isotropic and compressible, there are two characteristic waves above f_p, one real solution equal to approximately $K_{Po}\sqrt{\epsilon_E}$ and the other which is complex whose real part is approximately $K_{Eo}\sqrt{\epsilon_E}$. Below f_p, there is one wave number solution which is real and varies from nearly as large as K_{Po} near f_p to nearly as small as K_{Eo} when $f << f_p$. For the anisotropic, compressible plasma, there are again two characteristic wave number solutions above f_t, again one near K_{Po} and the other near K_{Eo}, while for $f < f_p$, one solution is obtained which rapidly decreases from a value on the order of the acoustic wave number to the order of the electromagnetic free-space wave number as $f << f_p$.

(b) The vacuum sheath case.

The effect of the vacuum sheath, besides resulting in real characteristic wave number solutions in frequency ranges where there may be none for the sheathless case, shifts the wave number in the direction of the EM free space wave number. Thus above f_t or f_p the wave numbers near K_E are increased in magnitude towards K_{Eo}, and for the compressible plasma the wave number near K_P is decreased in value towards K_{Eo}. Below f_t or f_p, the sheathless wave numbers are decreased in magnitude by the addition of the sheath in

the direction of K_{Eo}. This behavior is to be expected, since as the vacuum sheath is made thicker, the medium surrounding the antenna becomes more and more like free space and the wave behavior consequently also approaches the free space case.

References

Balmain, K. G. (1966), Impedance of a radio-frequency plasma probe with an absorptive surface, Radio Sci. Vol. 1, No. 1, 1-12.

Chen, K. M. (1964), Interaction of a radiating source with a plasma, Proc. of IEE (London) Vol. 111, No. 10, 1668-1678.

Chen, Y. and J. B. Keller (1962), Theory of the infinite cylindrical antenna including the feed point singularity in antenna current, J. of Res. NBS 66D, No. 1, 15-21.

Cohen, M. H. (1962), Radiation in a plasma III. Metal boundaries, Phys. Res., Vol. 126, 398-404.

Cook, K. R. and B. C. Edgar (1966), Current distribution and impedance of a cylindrical antenna in an isotropic compressible plasma, Radio Sci. Vol. 1, 13-19.

Fejer, J. A. and W. Calvert (1964), Resonance effects of electrostatic oscillations in the ionosphere, J. Geophy. Res., Vol. 69, No. 23, 5049-5062.

Hallen, E. (1963), Electromagnetic Theory, New York, Wiley.

Lee, S. W. and Y. T. Lo (1967), Current distribution and input admittance of an infinite cylindrical antenna in anisotropic plasma, IEEE Trans. AP-15, No. 2, 244-252.

Miller, E. K. (1967a, 1967b, 1967c), The admittance of the infinite cylindrical antenna in a lossy plasma: I The isotropic compressible plasma (Report No. 05627-10-S); II The anisotropic incompressible plasma (05627-11-S); III The anisotropic, compressible plasma (05627-13-S), U. of Michigan.

Seshadri, S. R. (1964), Radiation from an electromagnetic source in a half-space of compressible plasma-surface waves, IEEE Trans. Ant. Prop. AP-12, No. 3, 340-348.

Seshadri, S. R. (1965), Guided waves on a perfectly conducting, infinite cylinder in a magnetoionic medium, Proc. IEE (London), Vol. 112, 1497-1500.

Wunsch, A. D. (1967), The current distribution for a dipole antenna in a warm plasma, Spring URSI meeting, Ottawa, Ontario, Canada.

Errata 05627-14-S

Page 18 Second line below Eq. (8) now reads $K_E = 0.0285$,
should read $K_{Eo} = 0.0277$.

Page 18 Bottom line now reads $K_P = 33.1$,
should read $K_P = 33.8$.

Page 22 Interchange values of X on X = 5 and X = 2.5 curves on Fig. 4.

Page 41 Curve 4 should read X = 5 on Fig. 13.

Page 72, 73, 74; Equations (B4), (B6) and (B7). Replace the term $-iZ(2-N^2)$ by $-iZ$ and multiply the numerator by -1.